



AFRL-RB-WP-TR-2010-3029

**DESIGN AND ANALYSIS OF ADVANCED MATERIALS
IN A THERMAL/ACOUSTIC ENVIRONMENT**

**Delivery Order 0007: Volume 2-Risk-Minimized Structural Design
and Assessment for Reusable Launch Vehicles (RLVs)**

Ramana V. Granki, Jason King, and Matthew Riley

Wright State University

**MARCH 2010
Final Report**

Approved for public release; distribution unlimited.

See additional restrictions described on inside pages

STINFO COPY

**AIR FORCE RESEARCH LABORATORY
AIR VEHICLES DIRECTORATE
WRIGHT-PATTERSON AIR FORCE BASE, OH 45433-7542
AIR FORCE MATERIEL COMMAND
UNITED STATES AIR FORCE**

NOTICE AND SIGNATURE PAGE

Using Government drawings, specifications, or other data included in this document for any purpose other than Government procurement does not in any way obligate the U.S. Government. The fact that the Government formulated or supplied the drawings, specifications, or other data does not license the holder or any other person or corporation; or convey any rights or permission to manufacture, use, or sell any patented invention that may relate to them.

This report was cleared for public release by the Wright-Patterson Public Affairs Office and is available to the general public, including foreign nationals. Copies may be obtained from the Defense Technical Information Center (DTIC) (<http://www.dtic.mil>).

AFRL-RB-WP-TR-2010-3029 HAS BEEN REVIEWED AND IS APPROVED FOR PUBLICATION IN ACCORDANCE WITH ASSIGNED DISTRIBUTION STATEMENT.

*//Signature//

TRINA BORNEJKO

//Signature//

DAVID M. PRATT
Technical Advisor
Structures Division

This report is published in the interest of scientific and technical information exchange, and its publication does not constitute the Government's approval or disapproval of its ideas or findings.

*Disseminated copies will show “//Signature//” stamped or typed above the signature blocks.

REPORT DOCUMENTATION PAGE				Form Approved OMB No. 0704-0188	
<p>The public reporting burden for this collection of information is estimated to average 1 hour per response, including the time for reviewing instructions, searching existing data sources, gathering and maintaining the data needed, and completing and reviewing the collection of information. Send comments regarding this burden estimate or any other aspect of this collection of information, including suggestions for reducing this burden, to Department of Defense, Washington Headquarters Services, Directorate for Information Operations and Reports (0704-0188), 1215 Jefferson Davis Highway, Suite 1204, Arlington, VA 22202-4302. Respondents should be aware that notwithstanding any other provision of law, no person shall be subject to any penalty for failing to comply with a collection of information if it does not display a currently valid OMB control number. PLEASE DO NOT RETURN YOUR FORM TO THE ABOVE ADDRESS.</p>					
1. REPORT DATE (DD-MM-YY) March 2010		2. REPORT TYPE Final		3. DATES COVERED (From - To) 15 November 2006 – 30 March 2010	
4. TITLE AND SUBTITLE DESIGN AND ANALYSIS OF ADVANCED MATERIALS IN A THERMAL/ACOUSTIC ENVIRONMENT Delivery Order 0007: Volume 2-Risk-Minimized Structural Design and Assessment for Reusable Launch Vehicles (RLVs)				5a. CONTRACT NUMBER FA8650-04-D-3446-0007	
				5b. GRANT NUMBER	
				5c. PROGRAM ELEMENT NUMBER 0602201	
				5d. PROJECT NUMBER A0B7	
6. AUTHOR(S) Ramana V. Granki, Jason King, and Matthew Riley				5e. TASK NUMBER	
				5f. WORK UNIT NUMBER 0A	
				8. PERFORMING ORGANIZATION REPORT NUMBER	
7. PERFORMING ORGANIZATION NAME(S) AND ADDRESS(ES) Wright State University Department of Mechanical and Materials Engineering Dayton, OH 45435					
9. SPONSORING/MONITORING AGENCY NAME(S) AND ADDRESS(ES) Air Force Research Laboratory Air Vehicles Directorate Wright-Patterson Air Force Base, OH 45433-7542 Air Force Materiel Command United States Air Force				10. SPONSORING/MONITORING AGENCY ACRONYM(S) AFRL/RBSB	
				11. SPONSORING/MONITORING AGENCY REPORT NUMBER(S) AFRL-RB-WP-TR-2010-3029	
12. DISTRIBUTION/AVAILABILITY STATEMENT Approved for public release; distribution unlimited.					
13. SUPPLEMENTARY NOTES PAO Case Number: 88ABW 2010-1342, cleared 19 March 2010. Report contains color.					
14. ABSTRACT <p>Reusable launch vehicle (RLV) design is an inherently nonlinear, multi physics-based problem involving continuous, mixed, and integer optimization variables. With the wide presence of randomness in these variables, including epistemic, aleatory, and model-form uncertainties,, uncertainty in the problem must be accounted for in order to accurately quantify the system's probability of success.</p> <p>This research provides valuable tools to the RLV community by incorporating risk-minimization into the design of a vehicle. This has been accomplished by incorporating uncertainty quantification related to the aeroelastic and structural integrity of a launch vehicle, with a focus on flutter uncertainties.</p>					
15. SUBJECT TERMS reusable launch vehicle, risk-minimized design, flutter, epistemic, aleatory, and model-form uncertainties					
16. SECURITY CLASSIFICATION OF:			17. LIMITATION OF ABSTRACT: SAR	18. NUMBER OF PAGES 130	19a. NAME OF RESPONSIBLE PERSON (Monitor) Trina L. Bornejko 19b. TELEPHONE NUMBER (Include Area Code) N/A
a. REPORT Unclassified	b. ABSTRACT Unclassified	c. THIS PAGE Unclassified			

Table of Contents

LIST OF FIGURES	v
LIST OF TABLES.....	vii
FOREWORD	viii
GLOSSARY.....	ix
1.0 SUMMARY	1
2.0 INTRODUCTION.....	3
3.0 MISSION GOALS	5
3.1 Trajectory Optimization	5
3.1.1 POST and OTIS Comparison	6
3.2 FAST Trajectory Analysis	8
3.3 FAST Critical Mission Points	10
4.0 REUSABLE LAUNCH VEHICLE FINITE ELEMENT MODEL DEVELOPMENT	11
4.1 Structural Model Development	11
4.2 Structural Model Validation.....	16
4.2.1 Frequency Comparison Analysis	16
4.2.2 Modal Assurance Criteria Analysis.....	19
4.3 Aeroelastic Flutter Model Development	21
4.3.1 Reusable Launch Vehicle Aeroelastic Flutter Model	22
4.4 FAST Aeroelastic Flutter Analysis.....	24
5.0 RISK QUANTIFICATION.....	27
5.1 Aleatory Uncertainty Quantification.....	30
5.1.1 Monte Carlo Aleatory Uncertainty Quantification.....	34
5.1.2 First Order Reliability Methods (FORM)	35
5.1.3 Second Order Reliability Methods (SORM).....	39
5.2 Epistemic Uncertainty Quantification.....	43
5.2.1 Evidence Theory.....	43
5.3 Plausibility Decision	49
5.3.1 Sensitivity Analysis in Evidence Theory.....	55
5.4 Model-Form Uncertainty Quantification	59

6.0 OPTIMIZATION SCHEME	73
6.1 Reliability-Based Design Optimization Incorporating Evidence Theory	77
6.2 Particle Swarm Optimization	80
6.3 Adaptive Particle Swarm Optimization (A-PSO).....	87
7.0 FAST WING RESULTS.....	90
7.1 Aleatory Uncertainty Investigation	90
7.2 Epistemic Uncertainty Investigation	91
7.3 Reliability-Based Design Optimization Epistemic Uncertainty Investigation.....	98
9.0 BIBLIOGRAPHY.....	106

LIST OF FIGURES

Figure	Page
Figure 1: FAST Vehicle Tip-Tail Design	3
Figure 2: RLV Rocket Back Trajectory Analysis	9
Figure 3: High Fidelity RLV Structural Model	12
Figure 4: Original Configuration F Model.....	14
Figure 5: Modified Configuration F Model	15
Figure 6: First Five Natural Frequencies and Mode Shapes of the Original and Modified RLV FEA Wing Model.....	18
Figure 7: NASTRAN's RLV Wing Aerodynamic Model (Top) and Structural Model (Bottom)	23
Figure 8: RLV's Wing Flutter V-G Plot Representative (Mach 1.1, No Fuel, Sym. BC, 75° F).	25
Figure 9: RLV's Wing Flutter V- ω Plot Representative (Mach 1.1, No Fuel, Sym. BC, 75° F).	25
Figure 10: Flutter Dynamic Pressure with Symmetric Boundary Condition.....	26
Figure 11: Uncertainty Breakdown in Modeling Problems.....	27
Figure 12: Probability Density Function in 2D	30
Figure 13: Probability of Failure Representation.....	31
Figure 14: Graphical FORM Representation.....	37
Figure 15: Graphical Representation of FORM vs. SORM.....	39
Figure 16: Frame of Discernment	44
Figure 17: Basic Belief Assignment	44
Figure 18: Gas constant and Temperature BBA for Evidence theory Demonstration Case.....	46
Figure 19: Two Variable Hypercube Calculation	47
Figure 20: Two Variable Demonstration Case Function Evaluation.....	48
Figure 21: Two Variable Belief and Plausibility Calculations	49
Figure 22: PL and BEL Discontinues Behavior Based on Design Variable Modification.....	50
Figure 23: Plausibility Decision Behavior Based on Design Variable Modification	51
Figure 24: Plausibility Decision Methods.....	51
Figure 25: Two Variable Hypercube Demonstrating Plausibility Decision	52
Figure 26: Three Variable Hypercube Demonstrating Plausibility Decision	54
Figure 27: Four-Bar Truss Structure.....	55
Figure 28: Four-Bar Truss Structure BBAs	56
Figure 29: Reliability With Respect to X_1	57
Figure 30: Reliability With Respect to X_2	58
Figure 31: 2-DOF Wing.....	67
Figure 32: Real (Left) and Imaginary(Right) Components of $C(k)$ for 4 Models	69
Figure 33: Normal and Lognormal Plots of V_f	70
Figure 34: Vehicle Design Environment Framework.....	76
Figure 35: Gradient RBDO Flow Chart.....	77
Figure 36: Four-Bar Truss Structure.....	78
Figure 37: "Egg Crate Function" and Sample Iteration History	83
Figure 38: Number of Neighbors vs. Function Evaluations	85
Figure 39: Individuality and Socialability Factors vs. Function Evaluations	85
Figure 40: Number of Particles vs. Function Evaluations	86
Figure 41: Convergence Value vs. Function Evaluations.....	86
Figure 42: Model Design Space Reduction in A-PSO.....	89
Figure 43: NASTRAN FEA Wing Model for Aleatory Risk Quantification Analysis	90

Figure 44: Aeroelastic Analysis with Uncertainty Bound	93
Figure 45: Uncertainties for six variables	94
Figure 46: Composite Uncertainties Basic Belief Assignments	95
Figure 47: Aerodynamic Uncertainties Basic Belief Assignments.....	95
Figure 48: Six Variable RLV Problem Results.....	96
Figure 49: Simulation Time Six Variable RLV Problem	96
Figure 50: Variability Design of Skin Thickness Variables	99
Figure 51: BBAs for the Wing structure used in the RBDO study.....	100
Figure 52: Simulation Time RBDO Analysis	102

LIST OF TABLES

Table	Page
Table 1: RLV Wing Parameters.....	13
Table 2: Natural Frequency Comparison of Modified and Original RLV FEA Wing	16
Table 3: MAC of Original and Modified Models	20
Table 4: Monte Carlo Simulations Results	35
Table 5: UQ Results for a Closed-Form Problem.....	42
Table 6: Two Variable Plausibility Decision Results	53
Table 7: Three Variable Plausibility Decision Results	54
Table 8: Finite Difference Numerical Information	59
Table 9: Flutter Velocities for Four Models	69
Table 10: Distribution Parameters for Two Methodologies	70
Table 11: Distribution Parameters for Probabilistic Adjustment Factors Approach	71
Table 12: Four-Bar Truss Reliability Design Optimization Results.....	80
Table 13: “Egg Crate Function” Optimization results at standard parameters	84
Table 14: Aleatory Uncertainty Quantification Results Including Aeroelastic Analysis	91
Table 15: RBDO Wing Thickness Results	101

FOREWORD

The technical effort presented in this report was sponsored by the Air Force Research Laboratory, Air Vehicles Directorate under the STEAP Contract FA8650-04-D-3446, Delivery Order DO#7. The authors acknowledge the encouraging technical support provided by Ms. Trina Bornejko during the course of the project in which she served as the program manager. Dr. Jeff Zweber provided the initial guidance for this task during the beginning stages of the work.

The authors of this report wish to extend their appreciation to Dr. Jose Camberos and Dr. Mark Haney for their valuable ideas and guidance during the course of this work. The authors would also like to recognize Dr. Richard Snyder for providing us with the structural finite element model details.

The technical work on this task was accomplished under the leadership of the principal investigator, Ramana V. Grandhi. The principal investigator was assisted by Mr. Jason King and Mr. Matthew Riley.

GLOSSARY

AOA	Angle of Attack
A-PSO	Adaptive Particle Swarm Optimization
ASTOS	Aerospace Trajectory Optimization Software
ELV	Expendable Launch Vehicles
FAST	Future-Responsive Access to Space Technologies Program
FEA	Finite Element Analysis
FORM	First Order Reliability Method
GESOP	Graphical Environment for Simulation and Optimization
GTS	General Trajectory Simulation
MAC	Modal Assurance Criterion
OTIS	Optimal Trajectories by Implicit Simulation
PDF	Probability Distribution Function
POST	Program to Optimize Simulated Trajectories
PSO	Particle Swarm Optimization
RBDO	Reliability-Based Design Optimization
SORM	Second Order Reliability Method
USAF	United States Air Force
WPAFB	Wright Patterson Air Force Base
WSU	Wright State University

1.0 SUMMARY

Due to the rising cost of launching payloads into outer space and to address the problems of aging spacecraft, engineers are designing new vehicles that will reduce turnaround time and cost per launch. This activity has led to a large increase in research efforts conducted in the field of reusable launch vehicles (RLV). Vehicle design is an inherently non-linear, multi physics based problem involving continuous, mixed, and integer optimization variables. With the wide presence of randomness in these variables, including epistemic, aleatory, and model-form uncertainties, uncertainty in the problem must be accounted for in order to accurately quantify the systems probability of success.

This research provides valuable tools to the RLV community by incorporating risk-minimization into the design of a vehicle. This has been accomplished by incorporating uncertainty quantification related to the aeroelastic and structural integrity of a launch vehicle, with a focus on flutter uncertainties.

In this research a trajectory optimization was analyzed, from which critical flight points along the mission path were identified. To further investigate these critical points, a finite element structural and aeroelastic model was created to represent the RLV wing configuration. To ensure an accurate wing model, the model was validated based on a frequency and mode shape comparison analysis.

Aleatory uncertainty, epistemic uncertainty, and model-form uncertainty quantification techniques were explored for their suitability. To minimize risk associated with the variabilities in aeroelastic flutter, a reliability-based design optimization is considered in this investigation.

Three analyses were conducted on the FAST configuration F wing. The first analysis includes aleatory uncertainty in structural geometry. The second investigates epistemic uncertainty quantification incorporating evidence theory, where uncertainties in atmospheric conditions and composite materials were quantified. Finally, a gradient-based reliability design optimization was investigated, resulting in a weight reduction and increased structural reliability of the RLV's wing.

The technical contents of this report are organized in the following manner. Chapter 2 presents the background information for an RLV. Chapter 3 describes the mission trajectory analysis that served as the basis for defining critical aerodynamic loads. Chapter 4 discusses the development of the finite element model for the tip-tail FAST configuration F wing. Chapter 5 demonstrates techniques to quantify aleatory, epistemic and model-form uncertainty. Chapter 6 investigates reliability-based design optimization. Chapter 7 includes results for aleatory and epistemic uncertainty analyses of the FAST vehicle's wing as well as a reliability-based design optimization. The report then closes with Chapter 8 with concluding remarks.

2.0 INTRODUCTION

The United States now has an operating mixed fleet of space vehicles comprised of reusable space shuttle orbiters and expendable launch vehicles (ELVs). To reduce operational costs, launch vehicles must be designed to be reusable. In recent years the United States Air Force (USAF) and NASA have conducted ongoing research in the design of reusable launch vehicles (RLV) [1 - 6]. The US Air Force has been developing a reusable launch vehicle variously called Micro-X, Hot Eagle, and now FAST (Future Responsive Access to Space Technology). Configuration design activities for the FAST launch vehicle demonstrator have focused on configurations that have vertical tails on the wing tips as seen in Figure 1. This project seeks to develop and mature technologies that will allow development of future military launch vehicles that can land to launch another day.

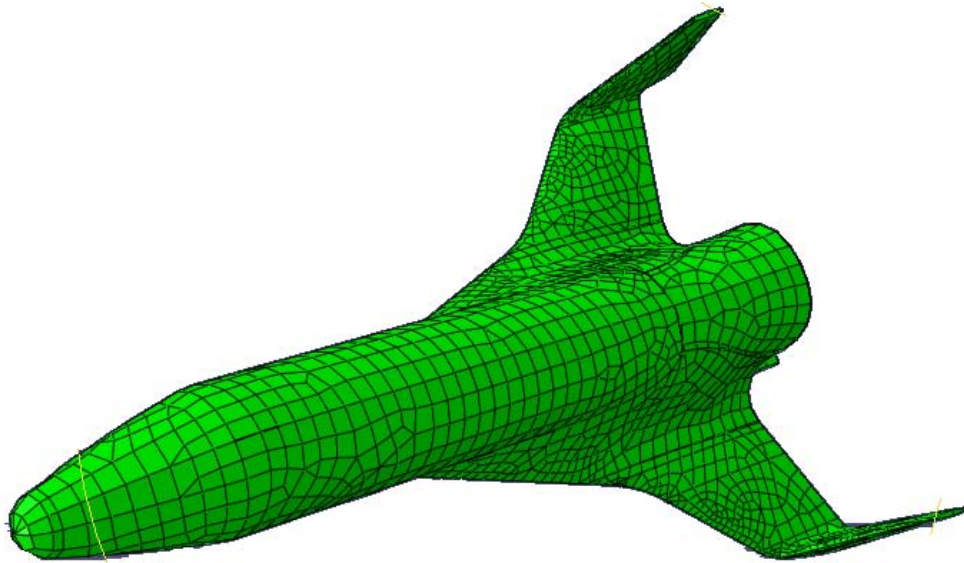


Figure 1: FAST Vehicle Tip-Tail Design

Future space access vehicle designs employ composite materials, thermal protection systems, health monitoring hardware, and propellant tanks to make the vehicles fully reusable and reliable. With many integrated subsystems, development of future vehicles with high reliability and confidence requires investigation of the interaction of multi physics behavior as well as optimization and quantification of the risk associated with each subsystem.

This technical effort with AFRL addresses two aspects of future vehicle design: First the work incorporates the vehicle trajectory by meeting the payload requirements at the systems level. Second at the subsystem level, this assessment conducts an aeroelastic flutter analysis which is used as a baseline to quantify and mitigate the risk in the aeroelastic flutter dynamic pressure. Flutter is an important characteristic for uncertainty quantification since this type of configuration is more apt to flutter at lower velocities which occur during the vehicles trajectory. The important goal of this assessment is to develop a toolbox which can be used to easily quantify different types of uncertainties. A spectrum of uncertainty quantification procedures must be incorporated in the design toolbox to consider probability distributions, parameter intervals, expert opinions, spatial and time-dependent variances, and limited experimental data in defining the subcomponent models. Through the use of advanced stochastic expansion techniques, the designer is supplied with the risks associated with, each of the selected alternatives. Some of the metrics of measure are the probability of failure, reliability, confidence bounds, belief plausibility, and sensitivity factors.

3.0 MISSION GOALS

The RLV mission goals are to examine how uncertainty propagates through system level traits to the subsystem level. The first step of this process is to identify a trajectory that the vehicle will follow, to complete a desired mission. In this chapter a trajectory optimization code was selected and executed based on the mission requirements of a reusable launch vehicle. Critical points along the trajectory were identified and transmitted into more detailed FEA simulations in the following chapters.

3.1 Trajectory Optimization

Trajectory is the path an object follows in order to reach a final destination. There are many different types of trajectories the FAST vehicle can travel [7, 8]. The trajectories can range from a downrange mission, where the vehicle launches from one site and lands at another, to a rocket-back and return to launch site. To begin vehicle design, a trajectory analysis is needed to determine what kind of flight loads the RLV will encounter during the mission. There are many codes available to solve trajectory optimization. Several codes include Optimal Trajectories by Implicit Simulation (OTIS), Program to Optimize Simulated Trajectories (POST), Graphical Environment for Simulation and Optimization/Aerospace Trajectory Optimization Software (GESOP/ASTOS), and General Trajectory Simulation (GTS). This research will focus on the most widely used and accepted trajectory optimization codes POST and OTIS.

3.1.1 POST and OTIS Comparison

Two trajectory optimization codes commonly accepted in the aerospace community are POST and OTIS. POST and OTIS represent the structural models of the launch vehicle with a generalized point mass. The programs are able to target and optimize point mass trajectories for an assortment of powered or unpowered vehicles. In a recent journal paper these two trajectory optimization codes were compared [9]. Physical and natural phenomena are modeled and calculated the same in both of the optimization programs. In theory each program should produce the same results given that they are both searching for an optimum. Any small discrepancies in the two optimization codes outputs can be attributed by the different mathematical optimizers and algorithms used during the analyses.

POST employs a gradient-based approach by integrating each point in the trajectory equation. During the analysis each point in the trajectory must satisfy all physical laws to move to the next point in the trajectory. OTIS has two methods to solve trajectory optimization, like POST it also contains a gradient-based approach as well as a collocation method. OTIS's collocation method allows more flexibility by giving the user the ability to choose the trajectory nodes and node spacing in the program. In theory an infinite amount of degrees of freedom could be examined, rather than the program choosing the points for the user. One drawback to this technique may not always produce an actual physical solution to the problem.

Both programs have a user interface where the optimization parameters are input. OTIS requires the user to define the continuity, that can lead to problems with inexperienced users.

POST automatically determines the continuity making it a more applicable program to optimize the FAST vehicle's trajectory.

Although the two programs seem very similar, POST appears to be more user friendly and straightforward. POST II was developed from the original POST software starting in 1995 and was written in FORTRAN 77 and C languages [10].

POST II's optimization procedure consists of:

- Inputting the data for all the phases
- Initialize equations of motion
- Propagating the trajectory until interrupted by the occurrence of the user-specified condition for the next event
- Restart equations of motion with the new inputs
- Repeat until final event and the post process the data

POST II can perform optimization targeting with or without inequality constraints, unconstrained optimization, and constrained (equal and/or inequality constraints) optimization. The program employs finite differencing to calculate the sensitivities of the optimization variable with respect to the constraints. The user selects the integration method and initial step size. The selection of the integration and step size are an important optimization consideration because it can make drastic impact on the computation time. POST II provides an automatic perturbation step size controller, although an initial guess is needed, it should make the loss of accuracy much

less than if a wrong perturbation variable was chosen, which can lead to introducing more uncertainty in the problem.

3.2 FAST Trajectory Analysis

In this research a trajectory optimization using POST was conducted on a nominal rocket-back mission. This type of mission requires the RLV to launch in a vertical position. Upon completing the mission the vehicle returns to the launch point and lands horizontally like a conventional aircraft, ready to be refueled and launched again in a short turnaround.

Figure 2 depicts the trajectory plot generated by POST II of the RLV's trajectory. This trajectory will supply essential information to complete finite element analysis at the critical points. A user specifies how the vehicle performs and the boundary conditions for a desired mission. POST II then solves the optimal trajectory based on the constraints and vehicle performance data. Boundary conditions include Mach number, final velocity, altitudes, and launch angles.

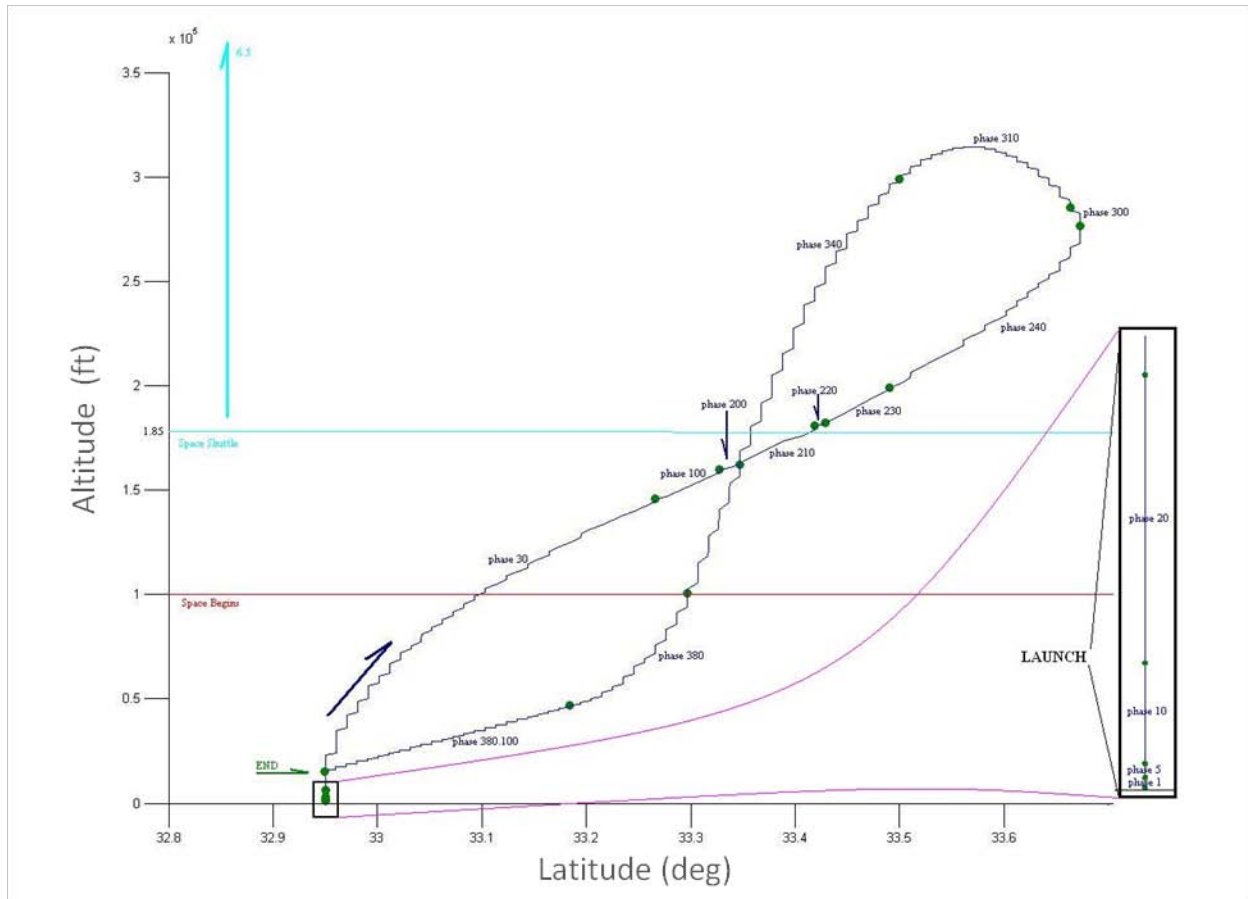


Figure 2: RLV Rocket Back Trajectory Analysis

The trajectory the RLV travels is explained. The vehicle starts from a vertical launch pad and launches. For a short duration, the vehicle continues vertically to reach the desired altitude and Mach number that defines the staging point. During this time the vehicle experiences heavy aerodynamic loading. For an operational, multi-stage launch vehicle additional stages would be located on the reusable booster. This would allow the vehicles to separate and continue on their desired mission. The propellant capacities for ascent propellant and rocket-back propellant were allocated to allow the vehicle to return to the launch site. After the launch vehicle and payload separates, the vehicles coast for a short time allowing them to have enough clearance to cause no damage. At this time the reusable booster will then pitch-over to an optimum altitude initiate for the reentry portion of the

trajectory. At the apex of the trajectory the vehicle changes orientation to allow for an optimal angle of attack (AOA) to reduce the temperatures the vehicle will encounter while entering the Earth's atmosphere. The vehicle then transitions to a maximum range glide altitude during the landing stage as it approaches the runway of the landing site.

3.3 FAST Critical Mission Points

Since the trajectory optimization program only explores the design space with a point mass, the performance analysis information obtained cannot be assumed to be exact. To quantify uncertainty of the vehicles performance, a higher fidelity analysis must be utilized using finite element analysis (FEA) approaches. Executing finite element analysis on the entire trajectory would be extremely computationally expensive. This calls for critical points along the trajectory to be recognized and analyzed. Critical points along the trajectory were identified during the trajectory, including: lift off, separation of the booster from the payload, the rocket back phase, reentry phase, as well as landing. At each of these critical points an assortment of finite element analysis techniques can be implemented depending on what scenario the vehicle is encountering, resulting in more accurate information for that specific flight point. For example a flutter analysis may be necessary at reentry or launching due to the vehicles experience in high dynamic pressures, knowing flutter can be affected by dynamic pressure. In contrary a maneuverability analysis may be conducted during the booster separation point or apex where the vehicle is making precise maneuvers, which may not be physically possible although the optimization program provides these as potential paths. These critical points will be analyzed using NASTRAN and ASTROS, finite element modeling packages that include aeroelastic analysis.

4.0 REUSABLE LAUNCH VEHICLE FINITE ELEMENT MODEL DEVELOPMENT

To fully analyze the reusable launch vehicle, representative models and simulations must be developed and implemented as tools in the design process. This chapter demonstrates the modeling techniques used to capture the RLV's wing structure as well as incorporating aeroelastic flutter analysis.

The RLV will have a tip-tail configuration presented in Figure 1. These configurations have advantages related to aerodynamic effectiveness of the tails during high AOA reentry, since they are not shadowed by the body. They also hold operability benefits in that the tails are away from the aft end of the vehicle and thus allow easier access to the engines. The tip-tail wings also offer the opportunity to mount a payload system on top of the vehicle without interference from the vertical tails.

4.1 Structural Model Development

It is important to be able to identify and quantify modeling errors introduced when different fidelity simulations are utilized. While high fidelity analyses generally produce solutions most reflective upon the actual scenario, the computational cost associated with these simulations can become restrictive within a design environment. Even for relatively simple designs, a large number of function evaluations, which in a simulation-based environment directly correlates to the number of simulations required and necessary for risk quantification and design optimization, are needed. Thus, it is important to be able to utilize lower fidelity

simulations where less accurate information is required, and only utilize high fidelity simulations in aspects of the design where more exact information is needed, such as using lower fidelity simulations in the initial exploration of the design space, and then utilizing the higher fidelity models as the design space is reduced.

4.1.1 Reusable Launch Vehicle Wing FEA Structural Model

Figure 3 is a high fidelity structural model developed by a highly regarded aircraft design company. This model was used as a baseline to create the wing structural model that will be used in the uncertainty quantification design process.

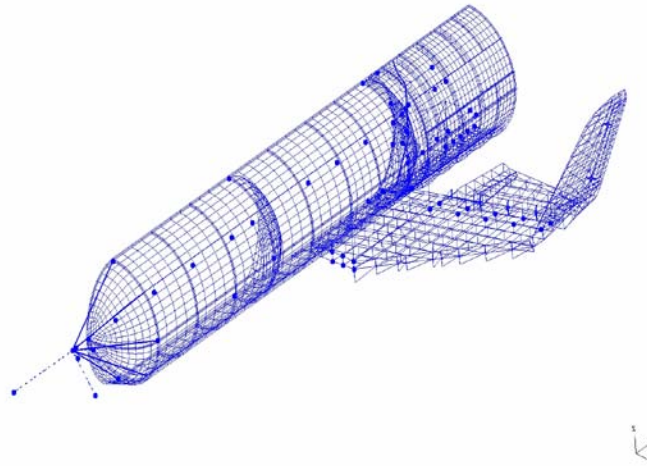


Figure 3: High Fidelity RLV Structural Model

The RLV's wing model was modeled based on the parameters found in Table 1. In this model, membrane elements with bending capability are used to represent the wing skins, shear panels represent the spars and ribs, and rod elements represent the posts. The center of gravity is maintained by adding non structured mass along the line of center of gravity axis.

Table 1: RLV Wing Parameters

Span	21.8 ft
Root Chord	18.2 ft
Tip Chord	6.1 ft
Mean Chord	13.1 ft
Aspect Ratio	1.8
Taper Ratio	0.333
Area Sref	265 ft ²
Sweep	48 deg
Dry Weight	800 lb

The structural model was developed in NASTRAN using the following elements.

Skins: QUAD-4/TRIA-3 Elements

Spars: Shear Elements

Ribs: Shear Elements

Spar Caps: Bar Elements

Figure 4 is an image of the RLV's wing obtained from full RLV structural model which will be referred to as the original model. The elements that construct the model in NASTAN can be found below Figure 4.

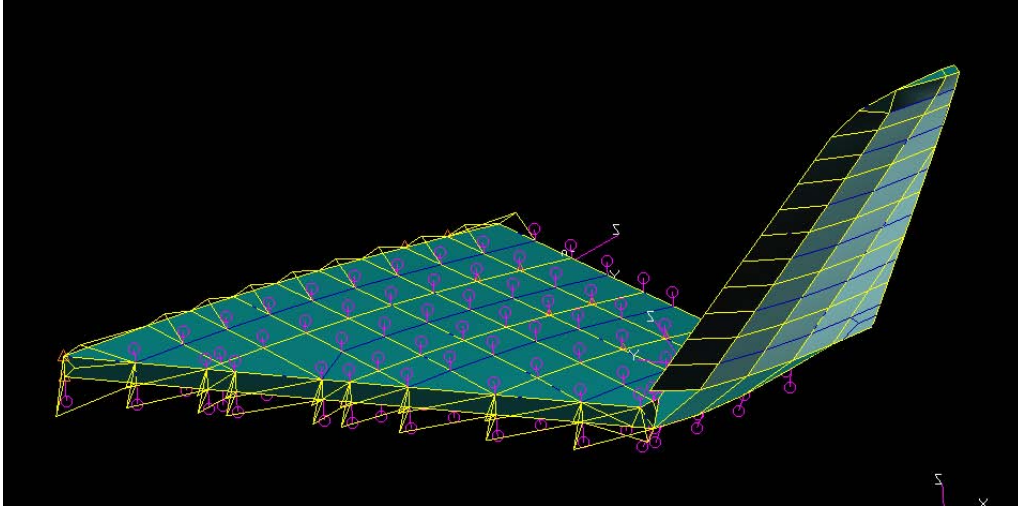


Figure 4: Original Configuration F Model

NUMBER OF GRID	POINTS	=	465
NUMBER OF CONM2	ELEMENTS	=	12
NUMBER OF CQUAD4	ELEMENTS	=	204
NUMBER OF CROD	ELEMENTS	=	605
NUMBER OF CSHEAR	ELEMENTS	=	174
NUMBER OF CTRIA3	ELEMENTS	=	28
NUMBER OF RBAR	ELEMENTS	=	133
NUMBER OF RBE1	ELEMENTS	=	5

To reduce the complexity of the original model, elements were removed to produce a more streamline model seen in Figure 5. The modified model of the RLV's wing will reduce the computational time when employing uncertainty quantification methods. Once again the elements used in the modified model can be found below the Figure 5.

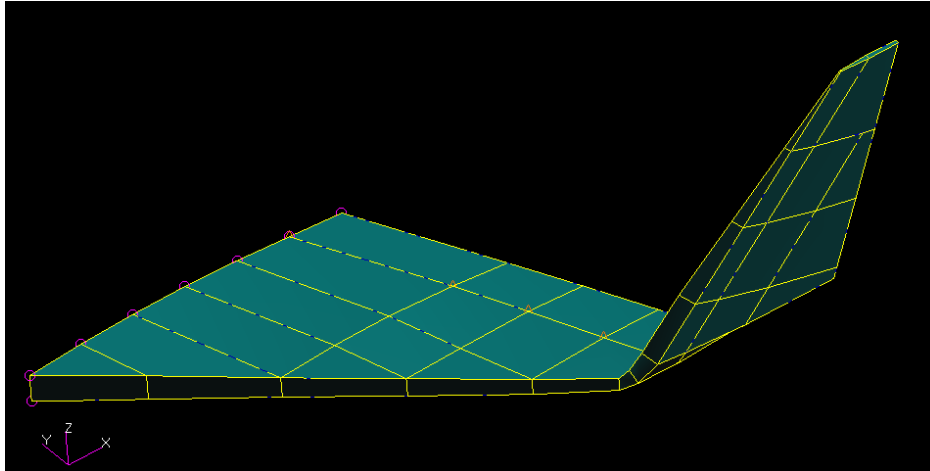


Figure 5: Modified Configuration F Model

NUMBER OF GRID	POINTS	=	91
NUMBER OF CONM2	ELEMENTS	=	5
NUMBER OF CQUAD4	ELEMENTS	=	54
NUMBER OF CROD	ELEMENTS	=	201
NUMBER OF CSHEAR	ELEMENTS	=	72
NUMBER OF CTRIA3	ELEMENTS	=	6

This modified model is capable of static and dynamic aeroelasticity simulations with possible analysis including:

- Static Analysis:
 - Divergent Dynamic Pressure
 - Trim Angle of Attack
 - Control Surface Reversal Pressure
 - Structural Displacement
- Dynamic Analysis:
 - Flutter Velocity
 - Low-frequency modes and mode shape

4.2 Structural Model Validation

When a model is modified from its original configuration it is necessary to know how the two models compare. To be able to use the modified model with confidence a validation study must be conducted. Two methods of validation were demonstrated in the following sections. The first validation implemented was a natural frequency comparison, where the two wing models first five natural frequencies were analyzed. The second validation uses the wing models mode shapes to investigate a modal assurance criterion analysis. Although both types of validation can be used separately a more conclusive comparison can be made when the two methods are coupled.

4.2.1 Frequency Comparison Analysis

The first validation analysis compared the natural frequencies between the two models described in section 4.1.1. The natural frequencies were established using NASTRAN's dynamic analysis. Both models were constrained at the root of the wing in all six degrees of freedom. Table 2 compares the models first five natural frequencies of the models.

Table 2: Natural Frequency Comparison of Modified and Original RLV FEA Wing

Mode	Original (Hz)	Modified (Hz)	% Difference From Original
1	7.79	8.02	2.95
2	16.89	12.57	25.5
3	23.63	26.16	10.70
4	57.38	54.88	4.35
5	76.15	72.27	5.08

The first five modes were selected to compare because in most cases the natural frequencies will most likely never reach above them in the physical world. Figure 6 illustrates the first five mode shapes and natural frequencies, where the figures on the left are the original wing configuration and the figures on the right are of the modified wing configuration. The first mode shape of the wing structures contains a bending mode. Whereas the second mode shapes illustrate a twisting modes. The third mode is a bending/twisting mode. The fourth and fifth modes are a combination of different mode shapes. Although the natural frequencies do not compare exactly some disagreement will occur when a lower fidelity model is introduced, due to the reduction of nodes.

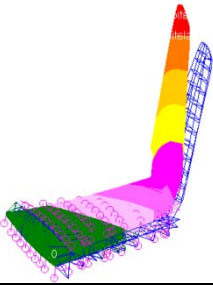
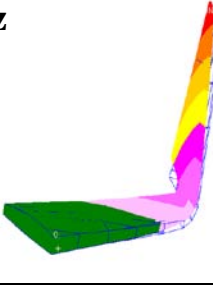
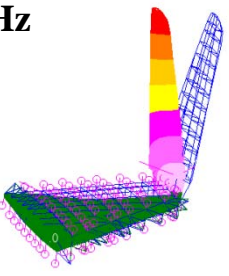
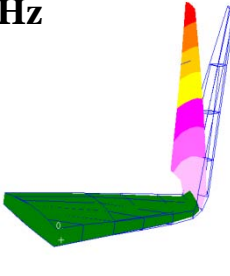
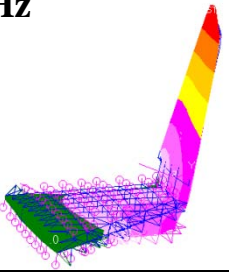
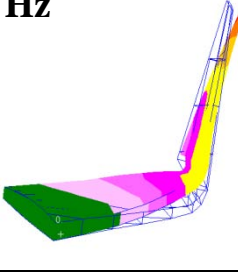
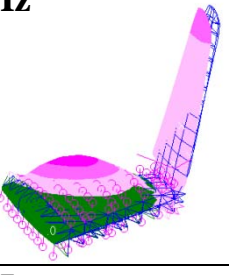
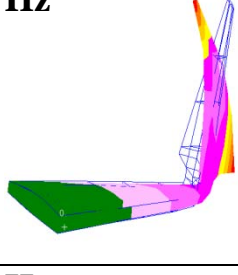
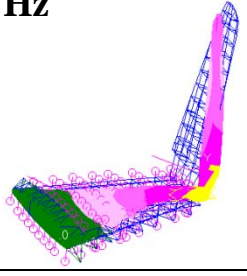
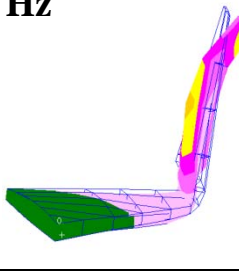
	Original FEA model	Modified FEA model
MODE 1	7.79 Hz 	8.02 Hz 
MODE 2	16.89 Hz 	12.57 Hz 
MODE 3	23.63 Hz 	26.16 Hz 
MODE 4	57.38 Hz 	54.88 Hz 
MODE 5	76.15 Hz 	72.27 Hz 

Figure 6: First Five Natural Frequencies and Mode Shapes of the Original and Modified RLV FEA Wing Model

4.2.2 Modal Assurance Criteria Analysis

Another important characteristic when comparing two models is to identify if the mode shapes demonstrate the same behavior. The modal assurance criterion (MAC) (Equation (1)) was the second method used to validate the new model. The MAC is a measure between two modes, whether they are by two experimental modes, a physic derived mode and experimental modes, or two physic derived modes [11, 12]. In most cases the MAC is used to compare a physical derived mode and an experimental mode. Since there is not a physical model of the RLV to get experimental modes the two finite element models were compared assuming the original model is exact.

$$\mathbf{MAC}(\boldsymbol{\psi}_l, \boldsymbol{\psi}'_l) = \frac{(\boldsymbol{\psi}_l^H \boldsymbol{\psi}'_m)^2}{(\boldsymbol{\psi}_l^H \boldsymbol{\psi}_l)(\boldsymbol{\psi}'_m^H \boldsymbol{\psi}'_{lm})} \quad (1)$$

The MAC matrix can be any size depending on how many mode shapes are being evaluated. In the MAC matrix each row and each column represent one mode shape. The MAC matrix consists of coefficients between 1 and 0, where a value of 1 indicates a perfect match and 0 indicated no similarity. If the two models were an exact match there would be 1s down the diagonal of the MAC. A value of .9 indicates a strong similarity between the two shapes. Mode switching can also be determined by the MAC matrix this can be seen by a high value located in an off diagonal.

The MAC was used to compare the first five mode shapes of the original and modified model. All six degrees of freedom of the mode shapes were compared. Table 3 contains the results of the MAC analysis.

Table 3: MAC of Original and Modified Models

	Original Model					
	Modes	1	2	3	4	5
Modified Model	1	0.979209	0.095065	0.256329	0.058633	3.80E-05
	2	0.057177	0.927935	0.21611	0.069353	0.000554
	3	0.240514	0.002087	0.867664	0.033638	0.368551
	4	0.001051	0.140134	0.002908	7.78E-06	0.737396
	5	0.034796	0.003098	0.002735	0.802372	0.013169

The table was color-coded to help distinguish the MAC coefficients. The boxes highlighted in red illustrate a good similarity between the two shapes. The first and second mode shape of the models compare very nicely, which can be seen by the values above .9 on the table. This is critical because when a flutter analysis is performed the first and second mode shapes are usually responsible for the flutter excitation (which will be described in a later section). The third mode shape is slightly less accurate but still correlates with the original model demonstrated by the .87 value in the diagonal. As described before in the previous section the third mode shape displays a bending/twisting motion. This can be seen in the blue boxes that there is around twenty percent correlation between the first, second, and third mode shapes. The fourth and fifth mode shape flip and can be seen with the high values found in the off diagonal located in the yellow boxes.

The two forms of validation that were investigated provides confidence, that the new model developed is an acceptable surrogate for the configuration F wing. It captures the physical model closely enough that the uncertainty quantification analysis can be implemented with meaningful data. The new model saves computational time while the uncertainty quantification

methods are being used and will allow a higher fidelity model to easily replace the model at the appropriate time of the design process.

4.3 Aeroelastic Flutter Model Development

Air vehicles that have vertical tails on the tips of the wing like the current RLV configuration are more susceptible to flutter due to the additional mass on the wing tip (which lowers bending frequency) and the additional aerodynamic lifting surface placed at the end of the wing. There have been many types of aeroelastic analysis conducted on hypersonic and reusable launch vehicles [13- 15]. This provides an excellent analysis to complete a risk quantification study using aeroelastic flutter as the failure bound (limit state).

To conduct an aerodynamic flutter analysis many inputs are needed for a simulation. The first input needed is a structural model that represents the vehicle being analyzed. Next, an aerodynamic model must also be constructed and positioned, to capture the aerodynamic loads associated with flight found in the trajectory optimization. In this section the steps taken to complete a series of flutter analysis on the RLV wing was conducted.

Aeroelasticity is a primary example of multi-disciplinary analysis. The coupling of aerodynamic and structural forces and responses are analyzed and the effects that this has on structural response, vehicle performance, and vehicle controllability are able to be determined. Performance parameters such as divergent dynamic pressures, control surface reversal pressures, trim conditions and flutter velocities can be calculated. Although aeroelastic analyses differ between Mach regimes the inputs and results to the analyses remain nearly identical for implementation within a design framework.

Flutter is a self-feeding vibration where aerodynamic forces on a wing couples with the natural mode of vibration to produce periodic motion that can cause catastrophic failure. The vibration movement of the wing increases an aerodynamic load which in turn drives the wing to deflect further. If the energy during the period of aerodynamic excitation is larger than the natural damping of the system, the level of vibration will increase. The vibration levels can thus build up and are only limited when the aerodynamic or mechanical damping of the object match the energy input, this often results in large amplitudes and can lead to rapid failure. This leads to an excellent parameter to examine with the tools for uncertainty quantification since there are so many uncertain variables that that could affect flutter.

4.3.1 Reusable Launch Vehicle Aeroelastic Flutter Model

NASTRAN FEA software was selected to construct the aeroelastic model due to the capability to perform linear aeroelastic analysis. NASTRAN's aerodynamic analysis, like structural analysis, is based on the finite element approach [16]. The finite aerodynamic elements are strips or boxes on which there are aerodynamic forces. These can be described simply by defining properties of the array (panel). The grid points defining the structure usually do not coincide with the grid points defining the aerodynamic elements, provision has been made to generate equations for interpolating between the two, known as splines. This interpolation is a key feature, since it allows the choice of structural and aerodynamic considerations to occur independently. NASTRAN provides three methods to complete a flutter analysis including the K, P, and PK methods. All of the flutter analysis presented in this research utilized the PK method. Choosing an appropriate aerodynamic theory is critical to compute a flutter analysis. NASTRAN

has implemented six aerodynamic theories including doublet-lattice subsonic lifting surface theory, ZONA51 supersonic lifting surface theory, subsonic wing-body interference theory, mach box method, strip theory, and piston theory. Doublet lattice and ZONA51 were both used in the flutter analyses given that only the subsonic and supersonic regimes were being analyzed. The Doublet-Lattice method can be used for interfering lifting surfaces in subsonic flow. ZONA51 is a supersonic lifting surface theory that accounts for the interference among multiple lifting surfaces. Figure 7 illustrates the structural and aerodynamic model developed in NASTRAN for the aeroelastic flutter analysis. The figure shows the aerodynamic model is the same shape as the structural model allowing for accurate interpolation between the two types of models.

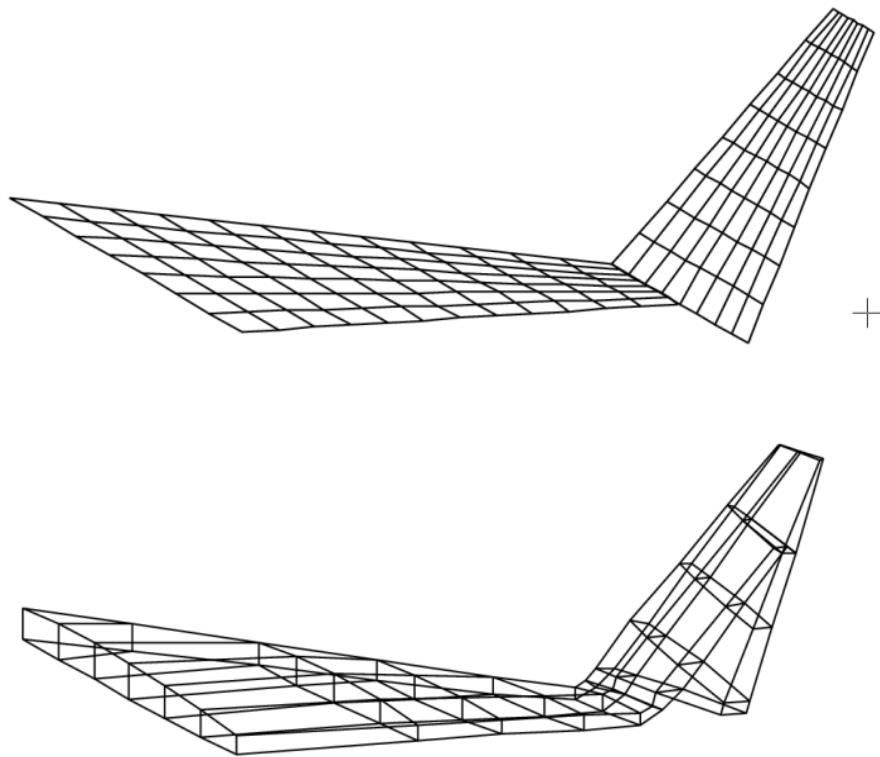


Figure 7: NASTRAN's RLV Wing Aerodynamic Model (Top) and Structural Model (Bottom)

4.4 FAST Aeroelastic Flutter Analysis

Figure 8 and Figure 9 illustrate the results for a single aeroelastic flutter case, in NASTRAN, of the modified RLV wing model, using Mach 1.1, at 75 deg F, and symmetric boundary conditions. The \circ represents the first bending mode, the \square is the second mode of the wing in torsion, and the \diamond is the third mode which consists of a bending twisting mode. Flutter occurs when one of the modes cross the zero axis in the V-G plot. The V-G plot in Figure 8 demonstrates the RLV's wing begins to flutter at 1500 ft/s. The two modes accountable for the flutter are the first wing bending and first torsion modes. Figure 9 reveals the coalescent behavior of the two modes to be around 1500 ft/s to 2000 ft/s, also confirming the flutter is occurring.

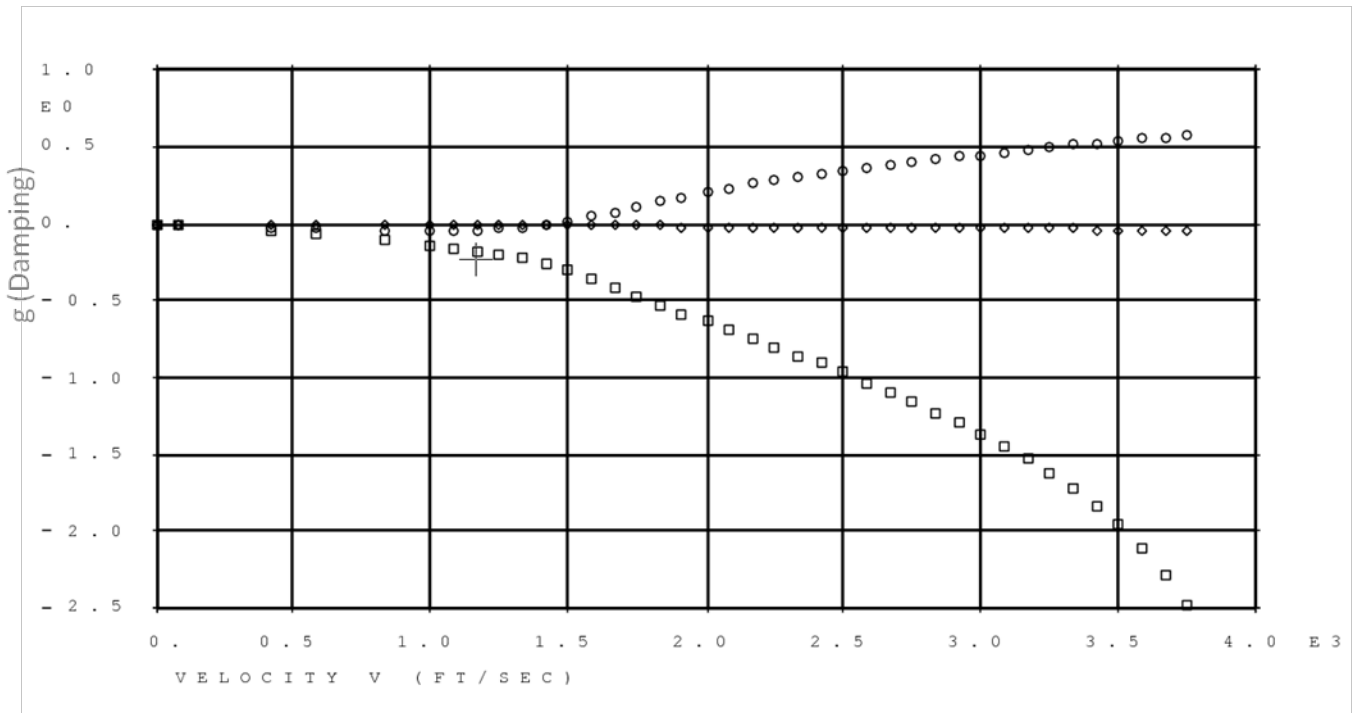


Figure 8: RLV's Wing Flutter V-G Plot Representative (Mach 1.1, No Fuel, Sym. BC, 75° F)

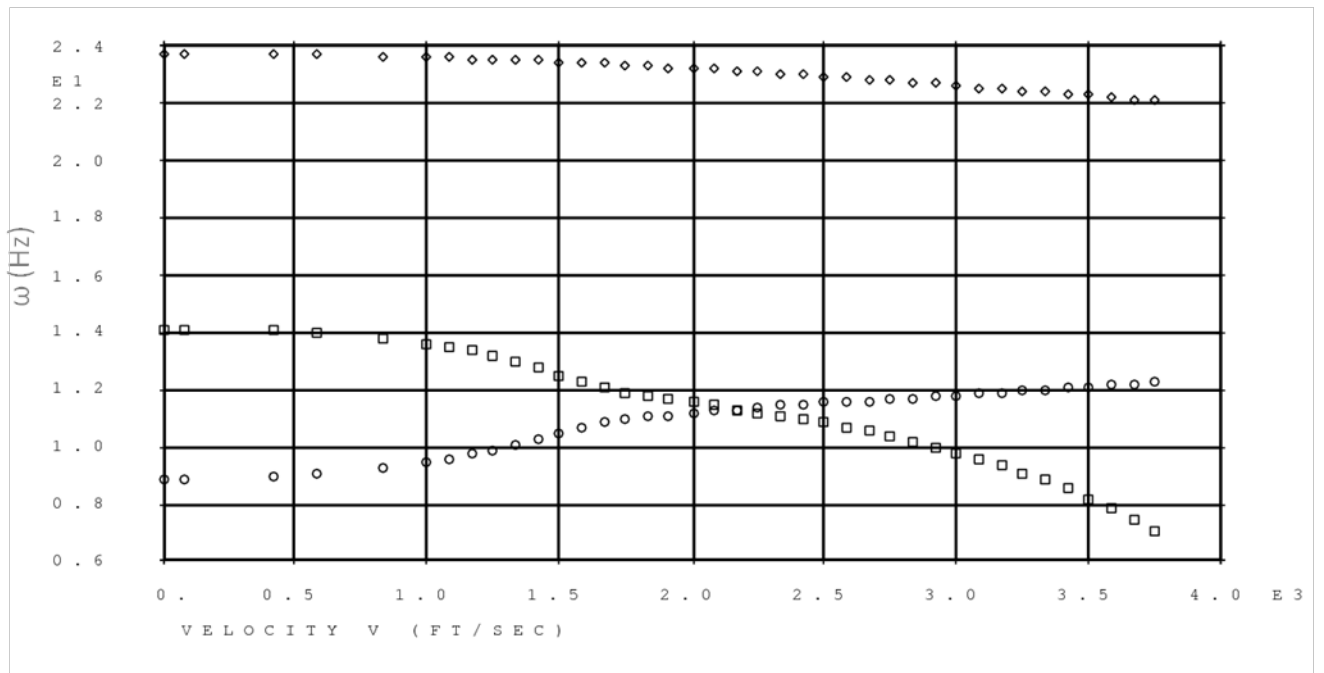


Figure 9: RLV's Wing Flutter V- ω Plot Representative (Mach 1.1, No Fuel, Sym. BC, 75° F)

To further explore the aeroelastic flutter of the RLV wing configuration a more in depth analysis was performed to make an assessment of flutter speed across the flight envelope using linear aerodynamic methods. This analysis will only be valid in the subsonic and supersonic regime due to the panel methods not being valid at transonic Mach numbers. This analysis will use the same initial conditions as stated in the previous aeroelastic flutter study, only changing the Mach number.

Figure 10 shows the results for the full flutter analysis. The lowest flutter dynamic pressure Mach number occurs at Mach 1.1. In this analysis the first mode shape was responsible for the flutter excitation in each of the simulations.

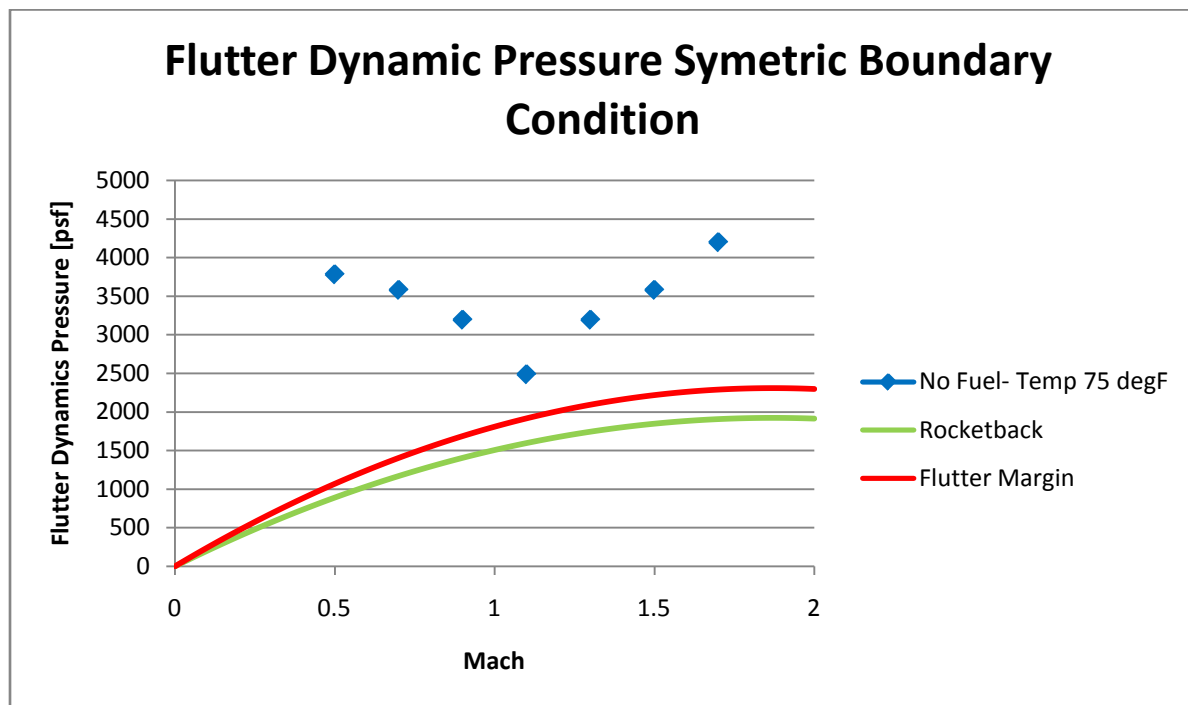


Figure 10: Flutter Dynamic Pressure with Symmetric Boundary Condition

5.0 RISK QUANTIFICATION

Uncertainty in a design problem can arise from multiple sources as stated by Rüdiger [17]. This is exacerbated in problems that involve modeling, whether that is a simplified physical model, or a computational model. These uncertainties can commonly associate with three distinct sources: Model-form uncertainty, parametric uncertainty, and predictive uncertainty. (Figure 11)

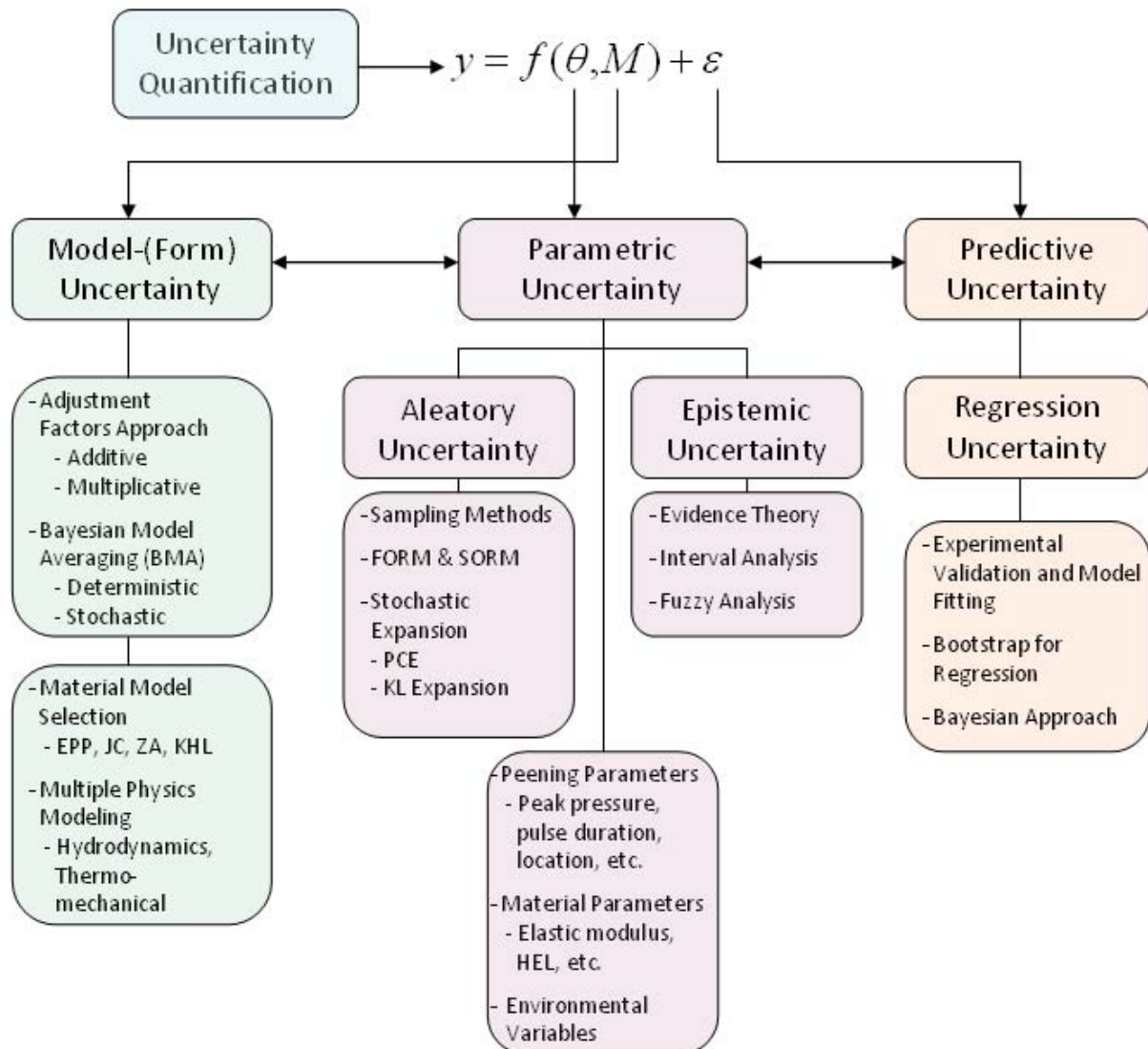


Figure 11: Uncertainty Breakdown in Modeling Problems

The significance of the uncertainty, and its source, is usually related to the confidence that a designer has in the models being utilized for analysis. As models are better understood, such as with static finite element analysis, the contribution to the overall uncertainty of both model-form uncertainty and predictive uncertainty are decreased, sometimes to the point of insignificance. However, in less understood phenomenon, or when working with over-simplified or novel models, the contribution to the total uncertainty of these two sources can potentially outweigh that of predictive uncertainty by orders of magnitude.

Parametric uncertainty refers to the uncertainty in the inputs to the model and analysis. Although models will usually operate with deterministic parameters in the scope of the actual physical manifestation of the problem, these values cannot always be considered deterministic. Inherent uncertainties can come from multiple sources, which contribute and compound to produce a degree of disbelief in the result of a single analysis. While uncertainties in the design variables and input parameters to a model are referred to in general as parametric uncertainty, the way in which these uncertainties are modeled and considered determines their further classification. Parametric uncertainty is expanded into aleatory and epistemic uncertainties [18].

When a physical problem is represented as a model, uncertainties are inherent to the modeling process. In aeroelastic design these uncertainties can arise from multiple sources, such as the input parameters into the model, the fidelity of aerodynamic analyses, and the aerodynamic and structural discretization of the physical domain. Extensive work has been completed in the past on parametric uncertainty on structural inputs [19, 20], aerodynamic inputs [20, 21], and environmental loading conditions [22]. However, the full uncertainty associated

with modeling consists of more than parametric input, but also includes other factors, such as the uncertainties introduced by the modeling process itself. The total uncertainty resulting from modeling can at a high level be broken into three distinct components [23]: model-form uncertainty—the degree of uncertainty between multiple models of the same physical problem—parametric uncertainty—the uncertainty in the parameters of an analysis—and predictive uncertainty—the unknown errors introduced by the simplifying assumptions of a model, often reduced to be the difference between a simulation result and the true physical problem (Equation (2)).

$$y = \tilde{f}_i(\bar{x}) + \hat{\varepsilon} \quad (2)$$

In Equation (2), $\tilde{f}_i(\bar{x})$ represents both the model-form and parametric uncertainty in the problem and $\hat{\varepsilon}$ represents the predictive uncertainty. Any uncertainty in the input vector \bar{x} is considered parametric uncertainty. While this uncertainty is propagated through the model, it is separable from model-form uncertainty in a well understood problem. The function \tilde{f}_i represents a model of the system. When multiple models are considered, the difference between the values of $\tilde{f}_i(\bar{x})$ is considered model-form uncertainty. Finally, the difference between the model's representation of the system, $\tilde{f}_i(\bar{x})$, and the “true” value of the analysis, y , is called the predictive uncertainty, $\hat{\varepsilon}$. The predictive uncertainty in a problem is a result of the assumptions made in the modeling process. Parametric uncertainty quantification methods and applications have been addressed in depth in the existing literature [19 - 22, 24 - 27]. However, the other two sources of uncertainty--both model-form and predictive uncertainty--are frequently ignored in aeroelastic problems.

5.1 Aleatory Uncertainty Quantification

Aleatory uncertainty is what is traditionally thought of when uncertainty is considered in a structural problem. It refers to the type of uncertainty where enough knowledge regarding the uncertainty of a parameter is known such that a continuous distribution function of its values can be determined and assumed to be valid. Aleatory uncertainty is typically defined in terms of probabilistic distributions (Figure 12).

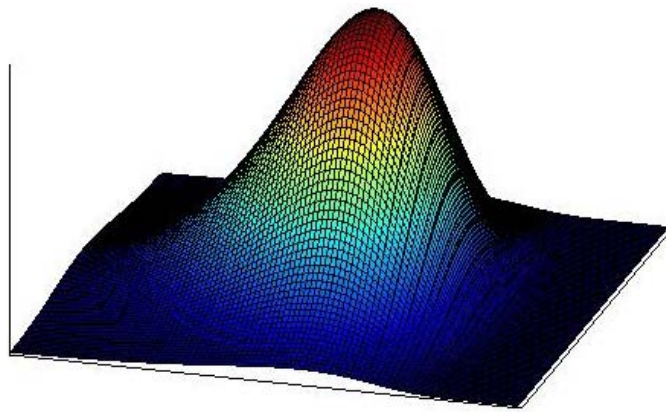


Figure 12: Probability Density Function in 2D

When described in this manner, a probabilistic distribution of output parameters can often be calculated, to which a probability of failure can be prescribed (Figure 13).



Figure 13: Probability of Failure Representation

However, all variables cannot always be assumed to be probabilistic. While with well understood parameters with an abundance of data available, it is possible to assign a distribution to the parameter, with other less understood parameters, this might not be possible, or might even result in erroneous results. If a probability is assigned to a value to which only limited data is available, it is possible to improperly define the variable, making the results of any analysis using that distribution, incorrect. Instead of assigning a distribution to these parameters in this case, another method must be explored for analyzing the uncertainty in these problems.

Aleatory uncertainty must be accounted for in the design process, while still maintaining computational efficiency. To quantify aleatory uncertainty quantification the following methods were explored.

- Monte Carlo Simulations
- First order reliability method(FORM)
 - Hasofer and Lind iteration method (HL)
 - FORM with adaptive approximations, TANA
- Second order reliability method (SORM)
 - Breitung's formulation
 - Tvedt's Formulation
 - Koyluoglu's Formulation

The goal of the preliminary analysis using aleatory uncertainty quantification techniques is to find a sufficient method of uncertainty quantification for the vehicle design, with specific interest initially in the aeroelastic design and analysis of an RLV wing. To complete an efficient uncertainty quantification analysis it is important that a method is selected that gives an accurate reliability with a minimal amount of function evaluations, which is directly related to simulation time. During the comparison of the aleatory methods, a closed form nonlinear equation was used to demonstrate the capabilities of the methods while not using computational time on executing FEA.

Each method listed above was analyzed and compared to a converged uncertainty quantification Monte Carlo Simulation analysis, which can be considered in this case to represent an “exact” solution, to show the relative accuracy of the reliability produced by each method.

During the analysis the function calls were also recorded to represent the number of aeroelastic simulations that would be required when a closed form equation will no longer be available.

The comparative study examines the different types of aleatory uncertainty quantification methods. With the results, a decision on which method provides the best accuracy taking into consideration of function calls for this demonstration. For example if a method has 99.9% accuracy and takes a month to execute the analysis compared to a method that has 97% accuracy that takes a week to execute, a sacrifice will have to be made on accuracy or time. This will provide the designer with information regarding the trade-offs between accuracy and computational time.

Equation (3) was selected as the closed form equation to demonstrate the potential of each method.

$$g(x) = x_1^4 + 2x_2^4 + x_1x_2 - 100 \quad (3)$$

The closed form equation represents a “black box” where any type of simulation can be placed. The closed form equation has two important characteristics that are congruent with an aeroelastic analysis. First, the closed form equation is highly nonlinear; both x_1 and x_2 are to the fourth power on behalf of the nonlinearity of an aeroelastic analysis. The second attribute of the equation is x_1 and x_2 are coupled, representing the coupling of variables between aerodynamic and structural portions of the aeroelastic analysis. Variables x_1 and x_2 both have a mean of 10 and a normal standard deviation of 5 throughout the comparison study. $g(x)$ represents the limit

state, which signifies the failure boundary, if the simulation results in a negative, it is considered a failure.

5.1.1 Monte Carlo Aleatory Uncertainty Quantification

Monte Carlo is one of the most basic sample techniques developed by Neuman and Ulam in 1949 known as a simple random sampling method. This technique can be implemented to solve uncertainty quantification analyses. To use the Monte Carlo Simulation technique, a distribution type is needed for the random variables. With the distribution type a random sample set is compiled. Using the values in the sample set as input values simulations are then executed. In most cases Monte Carlo simulation provides accurate results with very high computational cost. Using the random variables and closed form equation (Equation (3)), a Monte Carlo Simulation was performed using Matlab mathematical program to process the information.

The number of simulations was increased during each trial in the analysis to improve accuracy and demonstrate convergence. During each execution of the Monte Carlo simulation, the failures were recorded. The probability of failure was calculated by taking the number of failures and dividing it by the number of simulations as seen in Table 4.

Table 4: Monte Carlo Simulations Results

No. of Simulations	1,000	10,000	50,000	100,000	200,000	500,000	1,000,000	2,000,000	3,861,000
Number of failures	5	48	234	468	956	2379	4769	9476	18335
P_f (probability of failure)	0.005	0.0048	0.00468	0.00468	0.00478	0.004758	0.004769	0.004738	0.00474

Noting:

1. The number of simulations correlates to the accuracy of the Monte Carlo Simulation. As seen in Table 4 the probability of failure converges as more simulations are conducted.
2. A convenience of the Monte Carlo sampling technique is the process can be stopped and started at any time because each simulation is independent from the next.
3. Knowing each simulation is independent from the last, saved time in this comparative study.

The final simulation of the Monte Carlo technique employs 3,861,000 function evaluations. The analysis resulted in the probability of failure of 0.00474, and will be used as the most accurate uncertainty.

5.1.2 First Order Reliability Methods (FORM)

As seen in the results from the Monte Carlo Simulation, many simulations are needed to achieve a respectable solution; this provides motivation to find a more efficient method. First order reliability method (FORM) is an alternative technique to solve aleatory uncertainty

problems. FORM uses an iteration method while approximating the limit state function to solve for the probability of failure. Yan-Gang et al [28] demonstrated a general procedure for the first/second-order reliability methods will be used in this investigation.

Figure 14 graphically represents the FORM process. The first step in the process is the same as Monte Carlo, where the mean values, standard deviations, and distributions of the uncertain variables are required. In the figure μ_1 and μ_2 both have normal distributions. $g(x) = 0$ represents the limit state which separates the safe and failure region. FORM requires the means of the uncertain variables and the limit state function be normalized in this case using Equation (4) (X-space is transformed to U-space).

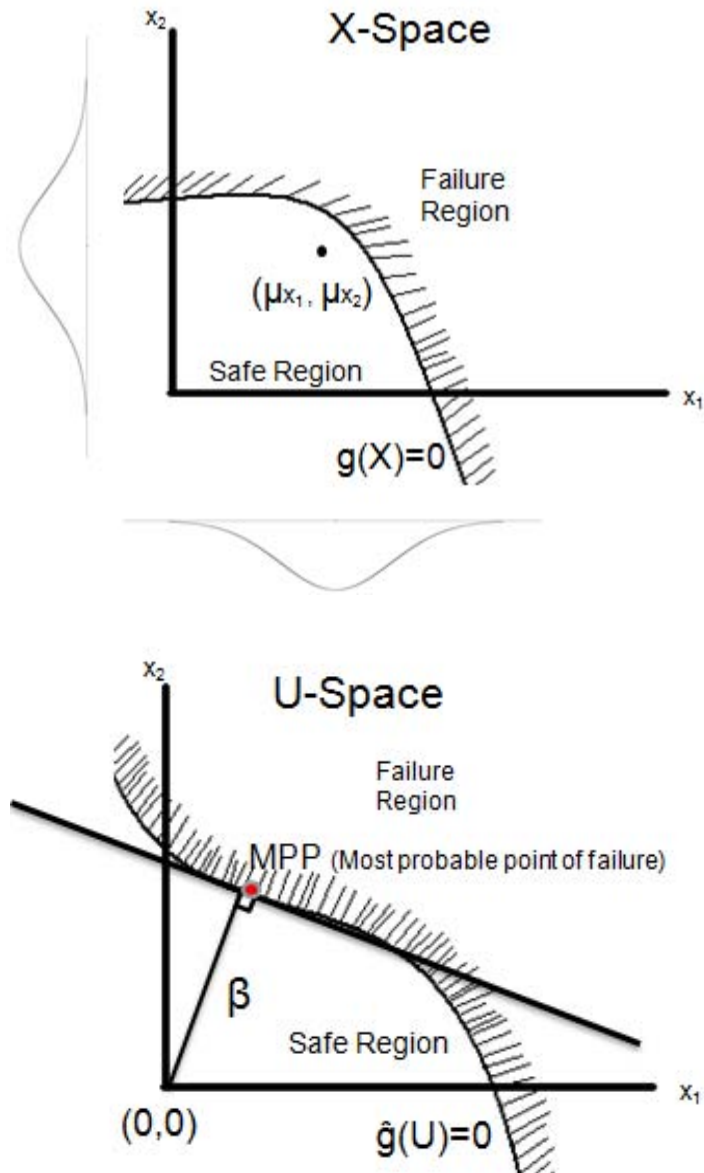


Figure 14: Graphical FORM Representation

$$u_i = \frac{x_i - \mu_{x_i}}{\sigma_{x_i}} \quad (4)$$

This transformation allows for the means of the uncertain variables to relocate to the origin (0, 0 position). Once transformed to U-space an optimization is preformed to minimize the length of β (reliability index). Where β contacts the limit state function the most probable point of failure is determined (MPP). A first order approximation can be made at the MPP. This approximation is illustrated by a line drawn tangent to the limit state function at the MPP. The reliability is then found by locating the correlating percent in a cumulative standard normal distribution table to determine the probability of failure. Two methods to solve FORM problems are Hasofer and Lind iteration method (HL) and FORM with adaptive approximations.

The Hasofer and Lind iteration method (HL) is a recursive algorithm used to solve reliability problems [29]. The HL method approximated the limit-state function using the first-order Taylor series.

FORM with adaptive approximation also approximates the limit state function using two-point adaptive nonlinearity approximation (TANA) Equation (5). Although extra function calls are needed initially to use TANA it closely approximates the limit state function resulting in less function calls to convergence [30].

$$G_T(U) = G(U_2) + \frac{1}{r} \sum_{i=1}^n u_{i,2}^{1-r} (u_i^r - u_{i,2}^r) \left(\frac{\partial g}{\partial u_i} \right)_{U_2} \quad (5)$$

5.1.3 Second Order Reliability Methods (SORM)

FORM works well when the limit state function is nearly linear. However, when considering aeroelastic limit state the function is not always linear. A second order reliability method (SORM) will tend to provide a more accurate representation of the design space. SORM requires the β and MPP from the FORM analysis. SORM calls for second order derivatives of the limit state function. On top of Figure 15 a first order approximation is shown. As observed in the graph the first order approximation underestimates the probability of failure by a significant amount, giving inaccurate results. On the bottom of Figure 15 a second order approximation is used to illustrate the improvement of the probability of failure approximation.

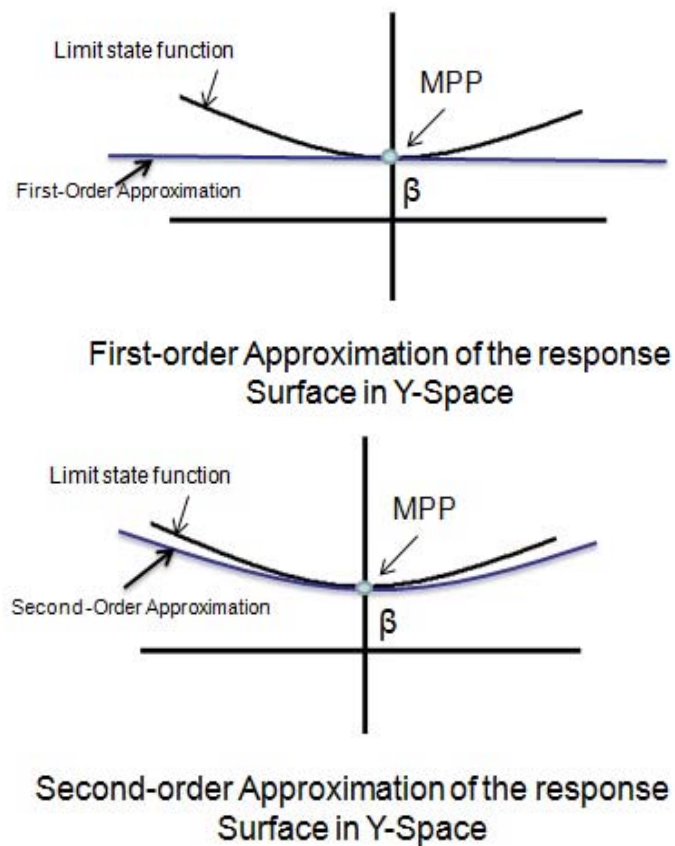


Figure 15: Graphical Representation of FORM vs. SORM

The first step of the process is to find β and the MPP in U space using a FORM method. The next step is to compute the second-order derivatives and create the B matrix which becomes very computationally expensive when more than two variables are being examined. The computational time can be reduced by using a function approximation (Such as TANA described in the previous section). Next the H matrix is created by rotating U space to Y space. This is completed by orthogonalizing the H matrix using the Gram Schmidt algorithm. Following with computing the main curvatures k_j by solving the eigenvalues of HBH^T . k_j and β is then used in each of the following methods to compute the probability of failure. The following SORM methods have a brief explanation and show the equations for the probability of failure.

Breitung's formulation was one of the first methods introduced in 1984 [31], Equation (6). The formulation is derived as an asymptotic formula of the failure probability.

$$p_f = \Phi(-\beta_f) \prod_{j=1}^{n-1} (1 + \beta_f k_j)^{-\frac{1}{2}} \quad (6)$$

Tvedt introduced a three-term approximation in 1984 in which A2 and A3 can be interpreted as the correction for Breitung's formula [32] Equation (7).

$$\begin{aligned}
p_f &= \Phi(-\beta_f) \prod_{j=1}^{n-1} (1 + \beta_f k_j)^{-\frac{1}{2}} + A_2 + A_3 \\
A_2 &= [\beta_f \Phi(-\beta_f) - \phi(-\beta_f)] \left\{ \prod_{j=1}^{n-1} (1 + \beta_f k_j)^{-\frac{1}{2}} - \prod_{j=1}^{n-1} (1 + (\beta_f + 1)k_j)^{-\frac{1}{2}} \right\} \\
A_3 &= (\beta_f + 1) [\beta_f \Phi(-\beta_f) - \phi(-\beta_f)] \left\{ \prod_{j=1}^{n-1} (1 + \beta_f k_j)^{-\frac{1}{2}} - Re \prod_{j=1}^{n-1} (1 + (\beta_f + 1)k_j)^{-\frac{1}{2}} \right\}
\end{aligned} \tag{7}$$

Koyluoglu and Nielsen developed Koyluoglu's formulation in 1994 making it a more recent method compared to the others [33] Equation (8). This formulation is a one-term approximation.

$$\begin{aligned}
p_f &= \Phi(-\beta_f) \prod_{j=1}^{n-1} \left(1 + k_j \frac{\phi(\beta_f)}{\Phi(-\beta_f)} \right)^{-\frac{1}{2}} \\
&\text{for } k_j > 0, j = 1, 2, \dots, n-1 \\
p_f &= 1 - \Phi(\beta_f) \prod_{j=1}^{n-1} \left(1 + k_j \frac{\phi(\beta_f)}{\Phi(\beta_f)} \right)^{-\frac{1}{2}} \\
&\text{for } k_j < 0, j = 1, 2, \dots, n-1
\end{aligned} \tag{8}$$

Using FORM and SORM methods, an uncertainty quantification analysis was accomplished on the closed form equation represented by Equation (3) using the same conditions that were used in the Monte Carlo simulation. The results of this comparative study can be found in Table 5. The gradients of the closed form equation are found using finite difference rather than mathematically solving for them to represent a black box simulation.

Table 5: UQ Results for a Closed-Form Problem

	Total Number of Function Calls	P_f	% Difference from MC
HL iteration method	87	0.01589	235.4
FORM with adaptive approximations	15	0.01590	235.4
Breitung's Formulation	21	0.00498	5.0
Tvedt's Formulation	21	0.00436	7.95
Koyluoglu's Formulation	21	0.00464	2.08
Monte Carlo	3,861,000	0.00474	0

The results from the aleatory uncertainty quantification methods were compared. The HL iteration method and FORM with adaptive approximation performed poorly as expected because the limit state function was nonlinear. FORM with adaptive approximations using TANA as the approximation shows a much faster convergence than the HL iteration method. The improvement of FORM with adaptive approximations finds an optimum β in 15 functions which is directly related to the amount of computation time that it would take when using this method for vehicle design. The FORM with adaptive approximations method will be used during the uncertainty quantification in vehicle design based on the savings of computational time.

Breitung's Formulation, Tvedt's Formulation, and Koyluoglu's Formulation were the three SORM methods compared. As explained earlier a FORM analysis is needed to construct

SORM. This makes SORM have a higher computational cost than FORM. Since the same method is used to solve for the Eigenvalue k that is used in the formulas the three methods have the same amount of function calls. For this particular problem Koyluoglu's Formulation performed closest to the Monte Carlo results.

5.2 Epistemic Uncertainty Quantification

In problems where little variable information exists, it is necessary to use an uncertainty quantification method that does not introduce additional assumptions, which would result in adding more uncertainty into the problem. These methods are referred to as epistemic uncertainty quantification methods. Epistemic uncertainty is uncertainty to which no assumptions are made regarding the parameters. Instead of defining a distribution to the parameters, intervals and bounds of parameters are assigned based upon limited available data, expert opinions, or prior knowledge of the problem. Using these interval definitions of variables, the uncertainty in the system must then be propagated using advanced methods. A known method of propagating this uncertainty is Dempster-Shafer Theory or Evidence Theory [34, 35].

5.2.1 Evidence Theory

A technique is needed to quantify uncertainty when there is little information known about the uncertain variables. Two epistemic variables that play a key role in a RLV are atmospheric conditions and composite properties. Evidence theory can quantify epistemic uncertainty without making any assumptions and was introduced to the reliability of structures by Bae et al [26, 36]. Evidence Theory measures uncertainty with two measures, belief (BEL)

and plausibility (PL). The reliability of the problem can be found between these two bounds. The upper bound is the plausibility and the lower is belief, this defines a probability interval. The bound size changes by the amount of information known about the uncertain variables. When little information is known the bound is large, contrary when full information is known the bound is small. To establish the values of BEL and PL a basic belief assignment (BBA) (Figure 17) needs to be constructed. To construct a BBA, first a frame of discernment needs to be established. The frame of discernment represents (Figure 16) all the possible distinct propositions given in Equation (9).

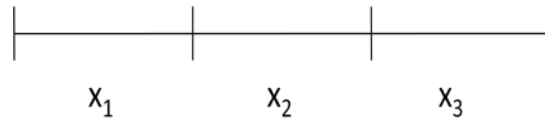


Figure 16: Frame of Discernment

$$2^X = \{\phi, \{x_1\}, \{x_2\}, \{x_3\}, \{x_1, x_2\}, \{x_2, x_3\}, \{x_1, x_3\}, X\} \quad (9)$$

Each combination in Equation (9) can be assigned a value from zero to one. This value will be referred to as m and is the weight of belief for that section of the frame of discernment.

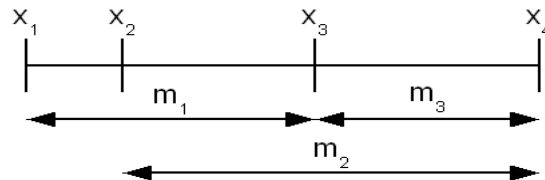


Figure 17: Basic Belief Assignment

The m contains the weighted information about the BBA and must satisfy Equations (10 - 12).

$$m(A) \geq 0 \text{ for any } A \in 2^X \quad (10)$$

$$m(\emptyset) = 0 \quad (11)$$

$$\sum_{A \in 2^X} m(A) = 1 \quad (12)$$

Using the BBA structure defined, Equations (13, 14) define $BEL(A)$ and $PL(A)$ respectively.

$$BEL(A) = \sum_{C \subset A} m(C) \quad (13)$$

$$PL(A) = \sum_{C \cap A \neq \emptyset} m(C) \quad (14)$$

To demonstrate evidence theory, a two variable case is provided based on an RLV wing flutter reliability. In this analysis the limit state is 2000 pounds per square foot (psf) flutter dynamic pressure. This states that if the flutter dynamic pressure falls below 2000 psf the analysis is considered a failure. Figure 18 denotes the two BBA's for the two variable demonstration case. The uncertain variables, temperature and gas constant, (which relate to the uncertainties with the air density) are considered epistemic variables because there is not enough accurate information to create a valid pdf. In this case the intervals were chosen by experts and the m was assigned by the expert's opinion.

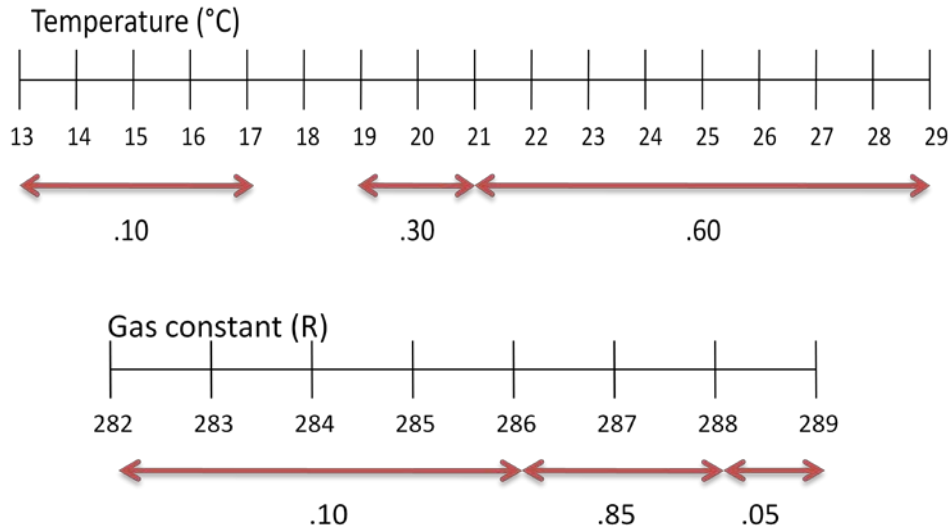


Figure 18: Gas constant and Temperature BBA for Evidence theory Demonstration Case

The next step is to combine the variables and complete the analysis. Figure 19 shows how the variables interact with one another. This is done by putting BBA's on the x and y axis. Lines are then drawn at each interval to show where the variables intersect. The intersections are represented by black dots. At each black dot a flutter analysis was executed with the corresponding inputs found on the x and y axis. This two variable problem shows, with the BBA's provided, 20 simulations will need to be executed. To calculate the BEL and PL hypercubes must be calculated. A hypercube in a two variable problem is represented by an area. For, example the yellow box in Figure 19 is a hypercube in which two of the intervals interact with one another. The area is then calculated by multiplying .6 by .1 which results in $m=.06$. The hypercubes must be calculated for each interaction.

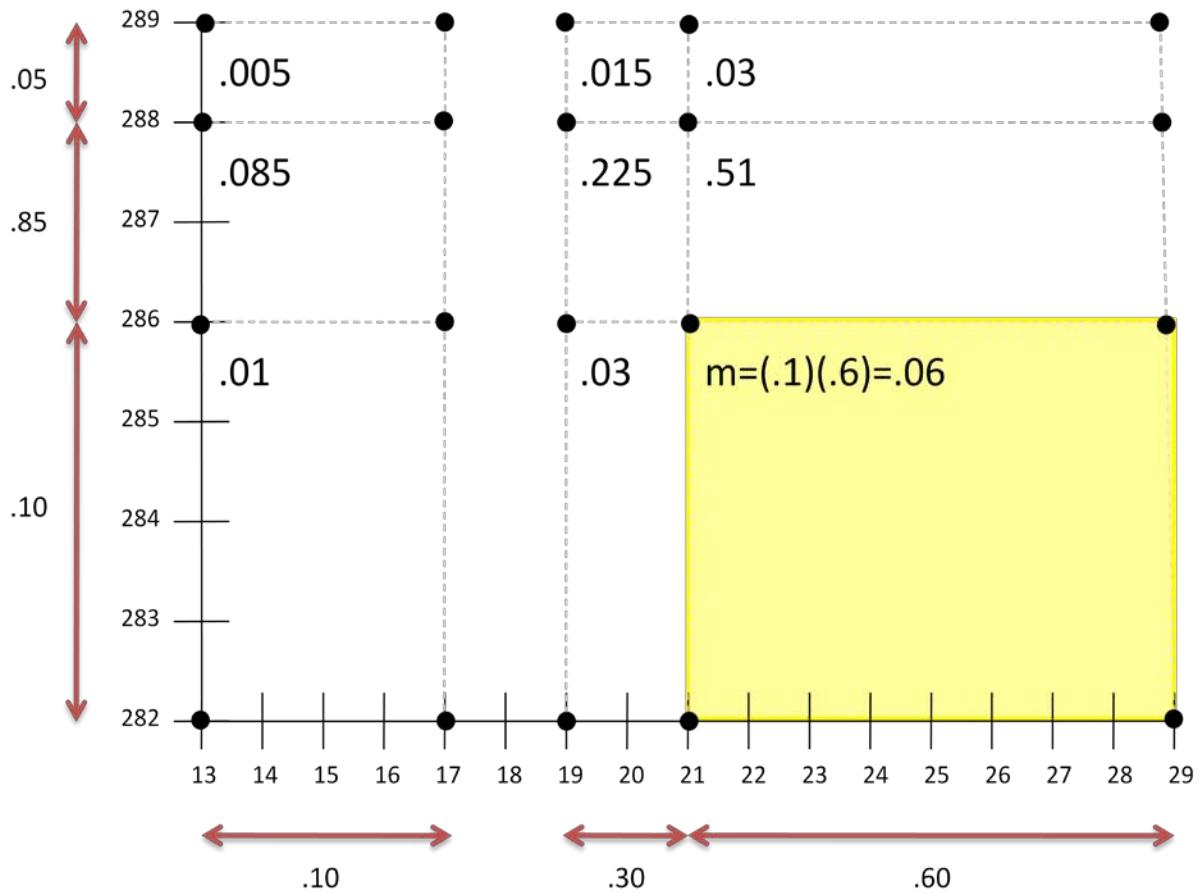


Figure 19: Two Variable Hypercube Calculation

Once the hypercubes are calculated the next step can be seen in Figure 20. The Flutter analysis was executed at each intersection. If the flutter analysis resulted in a flutter dynamic pressure less than 2000 psf the point was represented with a red dot. Likewise, if the flutter resulted in a dynamic pressure more than 2000 psf the intersection was represented with a blue dot.

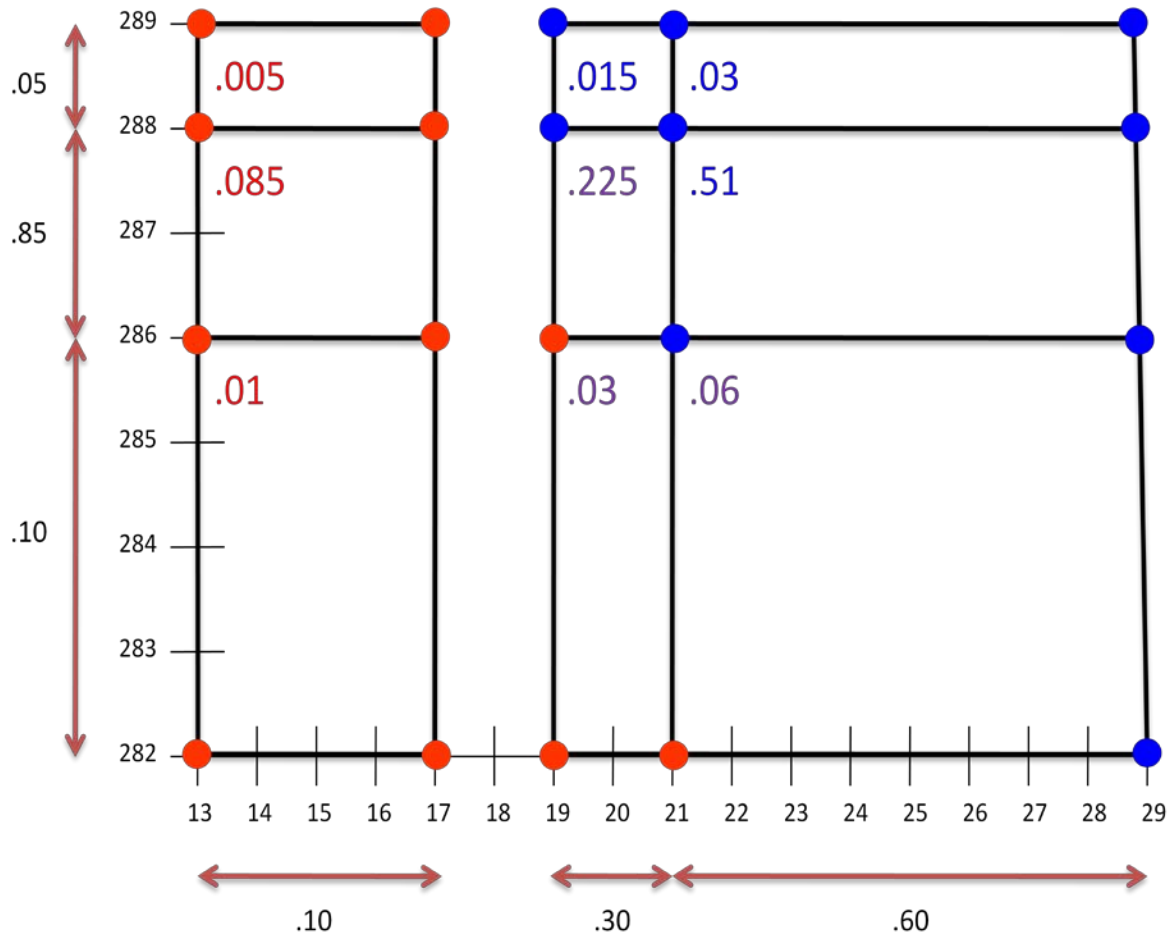


Figure 20: Two Variable Demonstration Case Function Evaluation

The BEL and PL can be calculated by examining Figure 20. If all of the intersections of a hypercube are blue then that hypercube is part of the BEL equation. If a hypercube has a combination of red and blue dots it falls in the PL section. PL also includes all of the hypercubes that were in the BEL equation. If a hypercube contains all red dots it is considered a failure region.

$$BEL(A) = \sum_{C \subset A} m(C)$$

$$BEL = .015 + .03 + .51$$

$$BEL = .555$$

$$PL(A) = \sum_{C \cap A \neq \emptyset} m(C)$$

$$PL = .015 + .03 + .51 + .225 + .03 + .06$$

$$PL = .87$$

Figure 21: Two Variable Belief and Plausibility Calculations

Figure 21 shows the calculation of BEL and PL. The BEL and PL are the bounds of the probability of success. This illustrates without making any assumptions that the reliability falls between .555 and .87.

5.3 Plausibility Decision

To accomplish the task of merging evidence theory into mathematical optimization procedures, sensitivity information of BEL and or PL metrics must be available with respect to the design variables. Design optimization using a search direction is one of the most basic methods of structural optimization. The most straightforward approach to obtain gradients, with respect to the design variables, is the finite difference method. As seen in Figure 22 a belief and plausibility demonstration is plotted with respect to a design variable. This shows even if finite difference was used there is little change in the belief and plausibility when the design variable is altered. The resulting gradients would always be a one or zero making gradient-based design optimization nearly impossible.

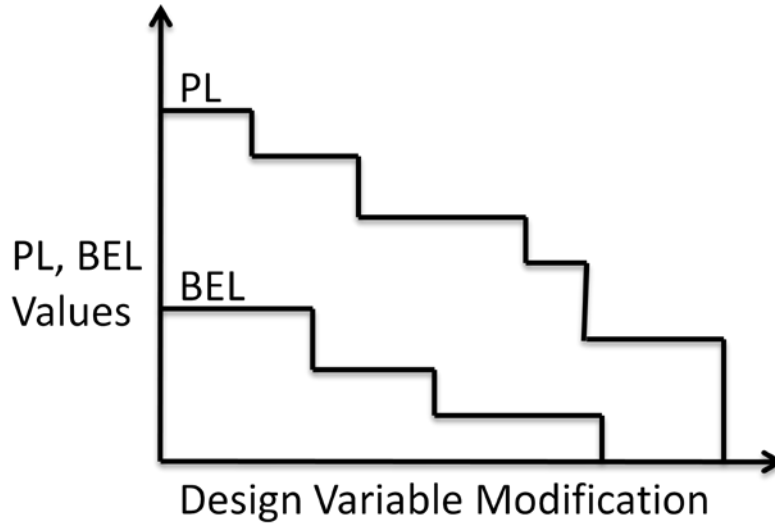


Figure 22: PL and BEL Discontinues Behavior Based on Design Variable Modification

To use gradient-based design optimization, a new measure must be determined. Bae introduced a new measure known as plausibility decision (PL_{dec}) [37]. Alyanak introduced an additional approximation method to find PL_{dec} [38]. This measure assumes a uniform probability distribution for each distinct proposition interval in the frame of discernment. Then the uncertainty is directly integrated, using approximation functions to increase efficiency. Since PL_{dec} is determined by integration, it creates a continuous measure that can be seen in Figure 23. Given that PL_{dec} is a continuous measure it will be possible to find gradient information that can be used in a finite difference method.

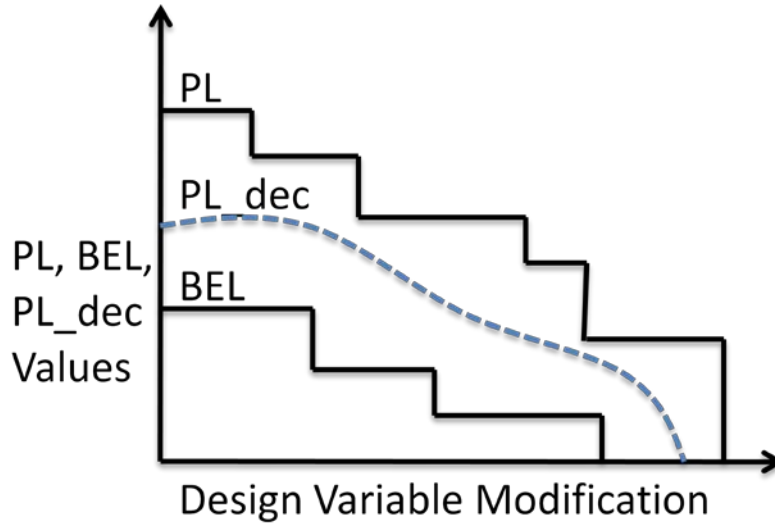


Figure 23: Plausibility Decision Behavior Based on Design Variable Modification

Three methods presenting the plausibility decision approximation can be found in Figure 24. On the left is the approximation developed by Bae in which the limit state function is approximated by using a nonlinear approximation (TANA). In the middle Alyanak developed a linear approximation that reduces computational time. Benanzer developed a numerical approximation where no extra simulations are required [39]. Benanzer plausibility decision method is an internal method used at Wright State University (Equation (15)).

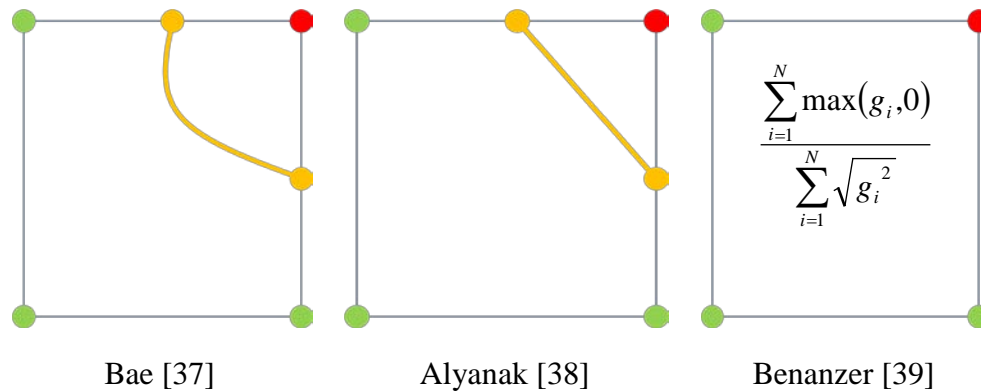


Figure 24: Plausibility Decision Methods

$$\frac{\sum_{i=1}^N \max(g_i, 0)}{\sum_{i=1}^N \sqrt{g_i^2}} \quad (15)$$

Each of the methods has previously been validated and can be implemented into a finite difference scheme to find the gradients of uncertainty quantification analysis. One major difference in the approximations is how they behave in an n-dimensional problem. The complexity of the approximation of PL_dec exponentially expands when more variables are used in Bae's and Alyanak's approximations. One advantage to Benanzer's plausibility decision approximation is it can easily be implemented into an n-dimensional problem, because the approximation is completed numerically. A validation of Benanzer's plausibility decision approximation using two uncertain variables in one hypercube that contains plausibility, can be seen in Figure 25 using Equation (16) as the limit state. The results of the actual and approximation plausibility decision can be found in Table 6. From this point onward Benanzer's plausibility decision approximation will be used in all of the uncertainty quantification analyses.

$$g(x_1, x_2) = 3 - \frac{18}{x_1} - \frac{6\sqrt{3}}{x_2} \geq 0 \quad (16)$$

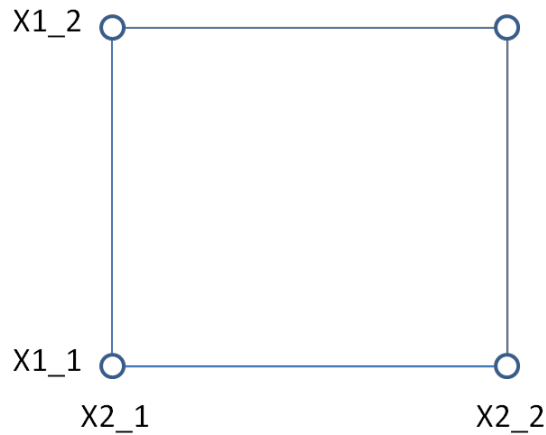


Figure 25: Two Variable Hypercube Demonstrating Plausibility Decision

Table 6: Two Variable Plausibility Decision Results

Simulation	x1_1	x1_2	x2_1	x2_2	Actual	PL_Dec	% Difference
1	9.3	9.7	9.3	9.8	0.2947	0.3155	7.05
2	9.2	9.5	9.1	9.5	0.9769	0.9425	3.52
3	8.9	9.6	8.7	9.8	0.8797	0.8512	3.24
4	8.7	10.3	8.8	10.8	0.3801	0.4374	15.07
5	8.3	9.3	8.8	11.8	0.7005	0.7371	5.22
6	8.8	9.1	10.1	11.7	0.26	0.2891	11.19

The comparison of the approximation and exact plausibility decision is located in Table 6. The assessment shows that the actual and PL_dec range from three to fifteen percent difference. Although this may seem high plausibility decision is calculated in each hypercube that contains plausibility meaning this approximation can over estimate in some and underestimate in others making them a close approximation for the entire evidence theory analysis. PL_dec is only an approximation and is used only to get a feel if the reliability of a system is close to the plausibility or belief bound.

To further expand the validation of Benazer's plausibility decision approximation three variables in one hypercube that contains plausibility will be validates and can be seen in Figure 26 using Equation (17) as the limit state.

$$g(x_1, x_2) = 3 - \frac{18}{x_1} - \frac{6\sqrt{3}}{x_2} - \frac{2}{x_3} \geq 0 \quad (17)$$

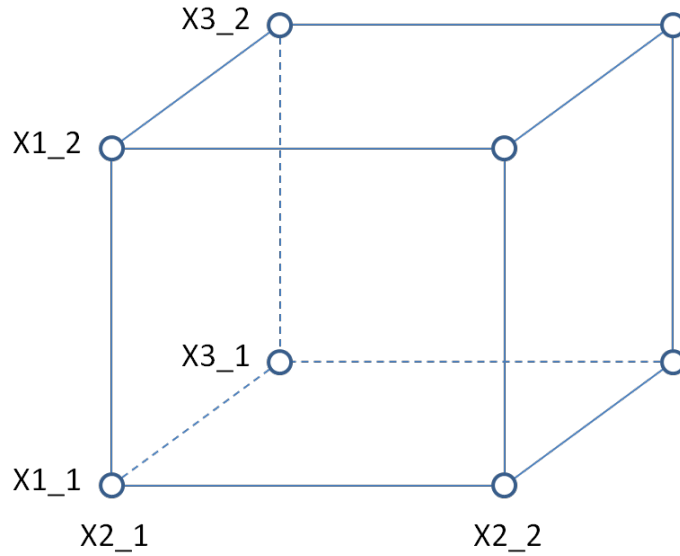


Figure 26: Three Variable Hypercube Demonstrating Plausibility Decision

Table 7 contains the results from the three variable demonstration case. Again this method produces a reasonable approximation. In simulation six it shows a twenty five percent difference of the approximation. Taking a closer look .1136 and .1428 are being compared. The approximation is only .0292 off of the actual, but since the values are so low the percent difference results in a large difference that is misleading.

Table 7: Three Variable Plausibility Decision Results

Simulation	x1_1	x1_2	x2_1	x2_2	x3_1	x3_2	Actual	PL_Dec	% Difference
1	9.1	9.7	9.2	9.9	25.1	25.9	0.9825	0.9566	2.64
2	9.3	9.9	9.2	9.9	22.3	25.4	0.8606	0.8397	2.43
3	9.2	10.1	9.2	9.7	21.3	31.4	0.7461	0.7745	3.81
4	9.7	12.1	7.4	8	8.4	9.7	0.9999	0.9964	0.35
5	10.3	13.1	7.9	9.3	7.4	10.2	0.4499	0.528	17.36
6	12.7	13.1	7.6	8.3	7.6	8.5	0.1136	0.1428	25.70

5.3.1 Sensitivity Analysis in Evidence Theory

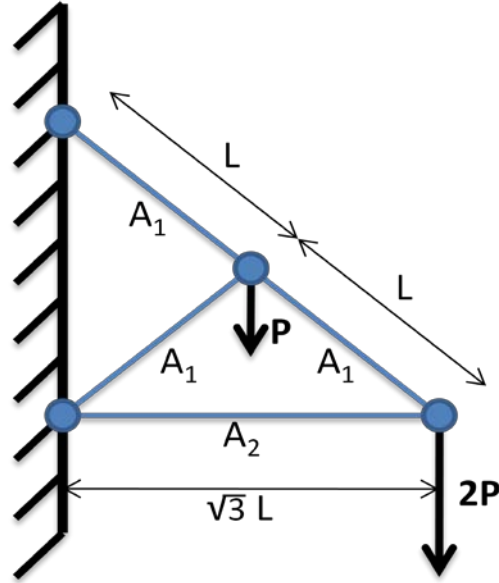


Figure 27: Four-Bar Truss Structure

To demonstrate a sensitivity analysis using evidence theory and PL_dec, a four bar-truss structure will be investigated (Figure 27). The four bar truss structure was developed by Haftka et al [40] to demonstrate a deterministic constrained optimization problem. The original problem has been modified to demonstrate plausibility decision and later reliability design optimization. There are three bars in the structure with the same length and cross sectional area A_1 and a final bar with cross sectional area A_2 . The modulus of elasticity is denoted by E , the load is P , and L represents the length of the beam. The constraint considered in this analysis is the displacement constraint situated at Equation (18) where $g(x) = \frac{6pL}{E} \left(\frac{3}{A_1} + \frac{6\sqrt{3}}{A_2} \right)$. When the problem is converted to a non-dimensional problem the limit state can be seen in Equation (19) where $x_1 = 10^{-3} \frac{A_1 E}{P}$ and $x_2 = 10^{-3} \frac{A_2 E}{P}$.

$$\delta \leq 10^{-3}L \quad (18)$$

$$g(x_1, x_2) = 3 - \frac{18}{x_1} - \frac{6\sqrt{3}}{x_2} \quad (19)$$

Using the BBAs seen in Figure 28 for the variables X_1 and X_2 a reliability analysis was conducted. Notice the BBAs are now in percentages. The percentages of the BBA are needed to perform the finite difference gradient evaluation.

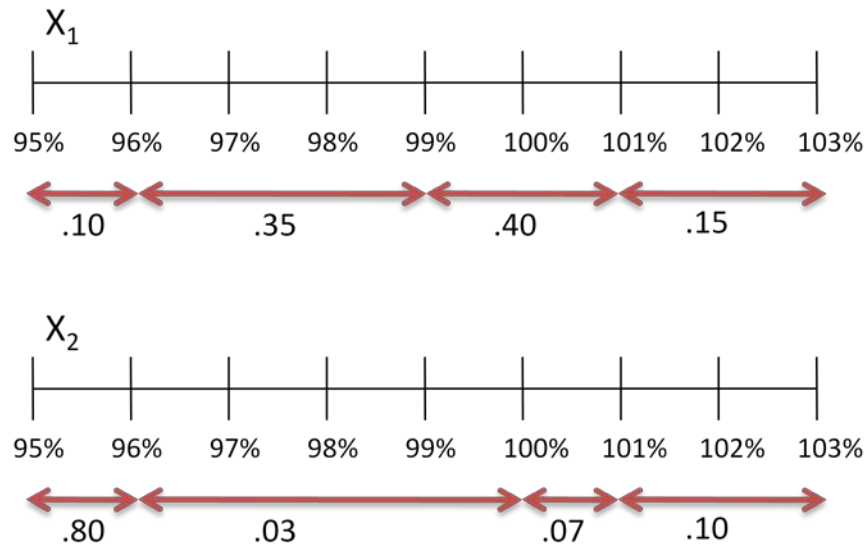


Figure 28: Four-Bar Truss Structure BBAs

To demonstrate the gradients of belief, plausibility, and plausibility decision with respect to the design variables of the displacement limit state, two parametric investigations were completed. This is completed by holding one of the design variables constant at the design condition and sweep the other design variable to determine the exact behavior of the measures

with respect to the design variable changes. The results can be found in Figure 29 and Figure 30 where the red line is the BL, the blue line is PL and the green dashed line is PL_dec.

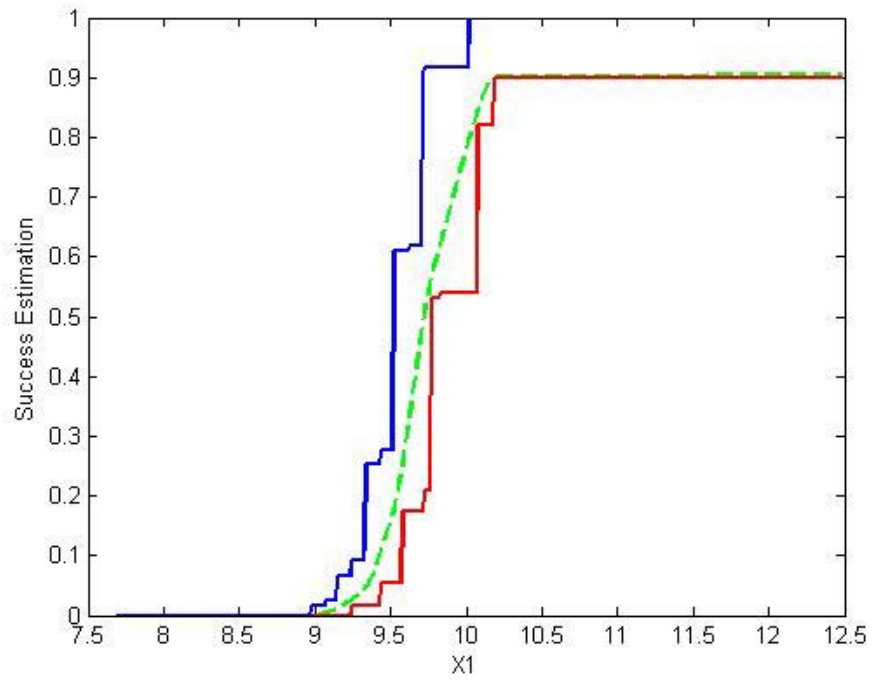


Figure 29: Reliability With Respect to X_1

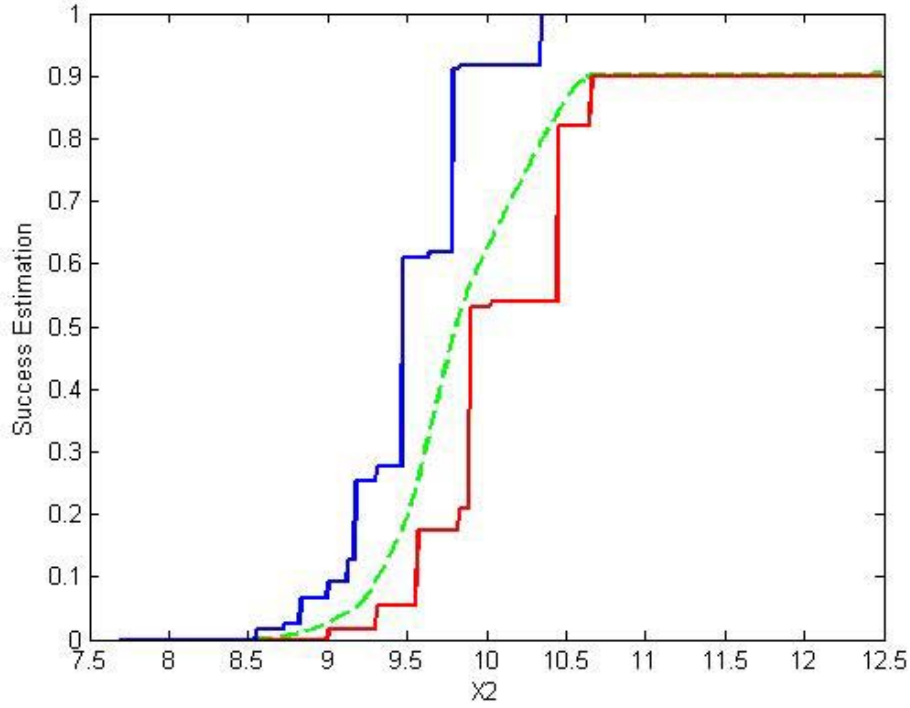


Figure 30: Reliability With Respect to X_2

The figures from the parametric study show that belief and plausibility are discontinuous. The plausibility decision is a smooth and continuous curve that falls between the belief and plausibility and gradient information can be used.

Now it is possible to complete gradient-based sensitivities using finite difference and plausibility decision. Equation (20) represents the gradient equation.

$$\frac{\partial Pl_{dec}}{\partial x_i} \quad (20)$$

Forward finite difference will be demonstrated on the four-bar truss structure. The three points ran in evidence theory using the four-bar truss structure can be found in Table 8.

Table 8: Finite Difference Numerical Information

Point	BEL	PL	PL_dec
(9.5, 9.5)	.0550	.2775	.1123
(9.6, 9.5)	.0550	.6095	.1975
(9.5, 9.6)	.0550	.2775	.1582

Equations (21, 22) show the gradients using finite difference with respect to the design variables X_1 and X_2 . From the results it can be seen that variable X_1 is almost as twice as sensitive as variable X_2 at this design point. This means X_1 has a much larger role in the design of the truss structure at this particular point.

$$\frac{\partial PL_{dec}}{\partial x_1} = \frac{.1975 - .1123}{9.6 - 9.5} = .8520 \quad (21)$$

$$\frac{\partial PL_{dec}}{\partial x_1} = \frac{.1582 - .1123}{9.6 - 9.5} = .4590 \quad (22)$$

5.4 Model-Form Uncertainty Quantification

When an analysis must be completed for an engineering problem, a representative model is often constructed to allow for analysis of the system. To construct this model, assumptions regarding the system must be made to simplify the problem to a level at which a model can feasibly and efficiently be constructed. These assumptions often vary between models and modeling packages, resulting in multiple solutions to identical problems. The difference between the multiple models of the same problem is representative of model-form uncertainty—the

uncertainty induced by the disagreement among multiple models of the same phenomenon. Because there are multiple models that give different answers to the same problem, a method must be utilized to combine these individual results into a unified solution while quantifying the uncertainty associated with this solution induced by the disagreement between the models. Multiple methods have been developed and implemented in the literature to quantify this model-form uncertainty, such as Bayesian Model Averaging [41] and the adjustment factors approach [42].

The adjustment factors approach was first demonstrated as a method to utilize expert opinions in Bayes' Theorem by Mosleh and Apostolakis [42] in 1986. This method uses an adjustment factor to modify the result of the best model. The adjustment factors approach has been demonstrated on multiple engineering problems by Zio and Apostolakis [43] and Reinert and Apostolakis[44].

The adjustment factor can be represented by multiple types of distribution—such as a normal or log-normal distribution—resulting in different adjustment factors being used. In the additive adjustment factor approach, the adjustment factor E_a^* is assumed to be a normal random variable. The representation of the adjusted model prediction is shown in Equation (23), where y^* represents the best model based on the expert opinion.

$$y = y^* + E_a^* \quad (23)$$

Knowing the results of multiple models, as well as their probabilities based upon the provided expert opinion, the means and variances of the adjusted model can be calculated by Equations. (24 – 27):

$$E(E_a^*) = \sum_{i=1}^N P(M_i)(y_i - y^*) \quad (24)$$

$$Var(E_a^*) = \sum_{i=1}^N P(M_i)(y_i - E(y))^2 \quad (25)$$

$$E(y) = y^* + E(E_a^*) \quad (26)$$

$$Var(y) = Var(E_a^*) \quad (27)$$

In the above equations, $E(y)$ represents the mean value of y , N is the total number of models considered, $P(M_i)$ represents the probability of model M_i based upon expert opinion, and y_i represents the prediction of model M_i . From the above equations, the mean and the standard distribution of the adjusted model y can be calculated and a normal distribution of the output can be constructed.

In the multiplicative adjustment factors approach, the adjustment factor E_m^* is assumed to be a lognormal random variable, and thus the adjusted model prediction is shown in Equation (28).

$$y = y^* * E_m^* \quad (28)$$

Assuming again that the results and the probabilities of the multiple models are known, the means and variances of the natural log of the adjusted model and adjustment factor can be calculated by Equations (29 – 32):

$$E(\ln|E_m^*|) = \sum_{i=1}^N P(M_i)(\ln|y_i| - \ln|y^*|) \quad (29)$$

$$Var(\ln|E_m^*|) = \sum_{i=1}^N P(M_i)(\ln|y_i| - E(\ln|y|))^2 \quad (30)$$

$$E(\ln|y|) = \ln|y^*| + E(\ln|E_m^*|) \quad (31)$$

$$Var(\ln|y|) = Var(\ln|E_m^*|) \quad (32)$$

The adjustment factors approach produces a statistical distribution of the adjusted model, accounting for the variation among the individual models. This distribution is dependent upon the expert opinion that goes into the model probabilities. The expert opinions are not infallible, and thus, an additional degree of uncertainty is introduced to the final distribution due to the uncertainty surrounding the model probabilities.

The uncertainty in the model probabilities can lead to multiple problems with the adjustment factors approach. Due to the weighting of the adjustment factors by the model probabilities, it is possible for the model probabilities to have significant effects upon the adjusted model. If changes in model probabilities lead to large changes in the adjusted model, the adjusted model becomes very dependent upon the model probabilities in addition to the variance among the models. Thus, it is critical to be able to identify the problems in which the adjusted model is sensitive to the model probabilities. To do this, the Modified Adjustment Factors Approach was developed in this work.

The probabilities, $P(M_i)$, assigned to each model are initially based upon expert opinion, or an incomplete set of preliminary data. The uncertainty involved in assigning these probabilities comprises the model uncertainty in the problem, and introduces an additional layer of uncertainty in to the output distribution, y . To propagate this uncertainty through to the distribution y , the values $P(M_i)$ are treated as uncertain variables with a defined normal distribution (Equation (33)).

$$P(M_i) = N(P(M_i)_{\text{exp}}, \sigma_{pm}) \quad (33)$$

While incorporating the distributions, the probabilities of each of the models must be constructed to still satisfy Equation (34).

$$\sum_{i=1}^N P(M_i) = 1$$

Such that

$$0 \leq P(M_i) \leq 1 \quad (34)$$

Due to the constraints of Equation (34), one model probability must be calculated based upon the results of the others. Due to the linear nature of Equation (34), though, if the standard deviations of all $P(M_i)$ are equal, the resulting distribution for the final model will still be a normal distribution around its mean value with the same standard distribution as the other models.

As $P(M_i)$ is no longer a deterministic measure, its uncertainty must be propagated through both adjustment factors approaches (Equations (24 - 27), (29 - 32)). By utilizing a Monte Carlo Sampling method, the statistical data regarding the final variable distribution can be calculated at individual model probabilities. These data points can then be combined to form a final distribution of the metric of interest which incorporates the uncertainty involved in the model probability selection. By comparing this new probabilistic adjustment factors approach distribution to the deterministic distribution calculated by a traditional approach, a rough sensitivity of the global problem to model uncertainty can be determined. This sensitivity can serve to guide further exploration in the reduction of model uncertainty through additional information—specifically detailing the need for posterior model likelihood updating.

While model-form uncertainty quantifies the discrepancies between models, parametric uncertainty quantifies the difference between a model and experimental data. Predictive

uncertainty is a result of the simplifying assumptions that are made in the construction of a model, such as an inviscid or incompressible flow assumption. Although individually, the models are deterministic, the presence of predictive uncertainty dictates that they should be instead described as distributions, to account for the known errors as a result of simplifying assumptions. To transform the deterministic solution to each model into a distribution, an assumption is made that each model's estimation contains a residual that is identically, independently and normally distributed (IDD), (Equation (35)).

$$\varepsilon_{ki} = y_i - f_k(x_i) \overset{IDD}{\sim} N(0, \sigma_k) \quad (35)$$

In Equation (35) y_i represents an experimental result at design variable vector x_i while $f_k(x_i)$ represents model k's solution at the same design variable vector. σ_k represents the standard deviation of the normal distribution, as calculated by Equations (36):

$$\sigma_k = \frac{\sum_{i=1}^n (y_i - f_k(x_i))^2}{n} \quad (36)$$

Now that the residual of each model is defined, the predictive distribution of each of the models can be constructed by adding the residual to the deterministic model prediction, as shown in Equation (37):

$$p(y | M_k) = f_k(x) + \varepsilon_k \quad (37)$$

Finally, the posterior likelihood of each model, $p(D | M_k)$, can be calculated by computing the joint probability of the experimental data as shown in Equation (38):

$$p(D | M_k) = p(y_1, \dots, y_n | M_k) = \prod_{i=1}^n p(y_i | f_k(x_i), \sigma_k) \quad (38)$$

The posterior likelihoods for each model calculated by Equation (38) can then be used to update the variable responses predicted by the adjustment factors approaches. This technique allows for further refinement of the model probabilities, $P(M_i)$, if deemed necessary by the probabilistic adjustment factors approach. As refinement requires the addition of experimental data, which can be expensive or even infeasible at an early design stage, it is crucial to utilize the sensitivity in the probabilistic adjustment factors approach to estimate the merit of adding additional data into the calculation of the model likelihoods.

To demonstrate the application of model uncertainty to an aeroelastic problem, a code was written that solves for the flutter velocity of a 2 degree of freedom—pitching and plunging—wing subject to unsteady aerodynamics (Figure 31).

$$C_1(k) = 1 - \frac{0.165k}{k - 0.0455i} - \frac{0.355k}{k - 0.3i} \quad (41)$$

$$C_2(k) = \frac{0.01365 + 0.2808ik - 0.5k^2}{0.01365 + 0.3455ik - k^2} \quad (42)$$

$$C_3(k) = \frac{J_1 - J_{oy}i}{J_1 - J_{oy}i + J_o - J_{1y}i} \quad (43)$$

$$C_4(k) = \frac{(1 + 10.61ik)(1 + 1.774ik)}{(1 + 13.51ik)(1 + 2.745ik)} \quad (44)$$

Where k is the reduced frequency of the system defined by Equation (45) where ω is the frequency of oscillation of the airfoil and U_∞ is the free-stream velocity

$$k = \frac{\omega^* b}{U_\infty} \quad (45)$$

The real and imaginary part of these four surrogate models vary over an average operating range of k 's, as shown in Figure 32.

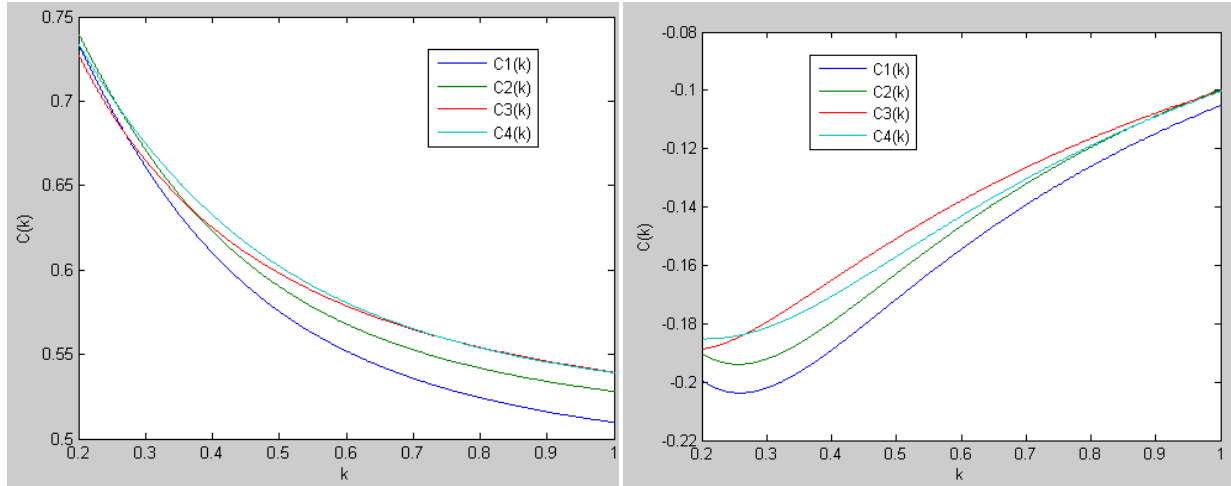


Figure 32: Real (Left) and Imaginary(Right) Components of $C(k)$ for 4 Models

Once a surrogate model of Theodorsen's Function is decided upon, the flutter velocity for this system of equations can then be solved using the theory of unsteady aerodynamics (Equations (39 - 40)) and the V-g Method. However, due to the multiple possible surrogate models to use, there is inherent model uncertainty to the problem. Executing the V-g method for the sample 2 DOF wing produced results shown in Table 9.

Table 9: Flutter Velocities for Four Models

	Vf (ft/s)	Model Probability
C1(k)	101.393	0.3
C2(k)	99.469	0.15
C3(k)	97.968	0.4
C4(k)	97.598	0.15

By assigning a probability to each of the four models, based on expert opinion, an adjustment factors approach can be utilized to develop a distribution of the flutter velocity for the

2 DOF system. By using the additive and multiplicative adjustment factors approach detailed in the sections above, a normal and lognormal distribution of the flutter velocity can be developed. Table 10 shows the means and standard deviations of the figure of merit—in this case the flutter velocity of the system—for both the additive and multiplicative adjustment factors approach. These distributions are then plotted in Figure 33, showing the probability density functions for the flutter velocity of the wing as calculated by both the additive and multiplicative adjustment factors approach.

Table 10: Distribution Parameters for Two Methodologies

	Mean	Standard Dev.
Additive (normal)	99.16515	1.5635
Multiplicative (lognormal)	99.15289	1.55687

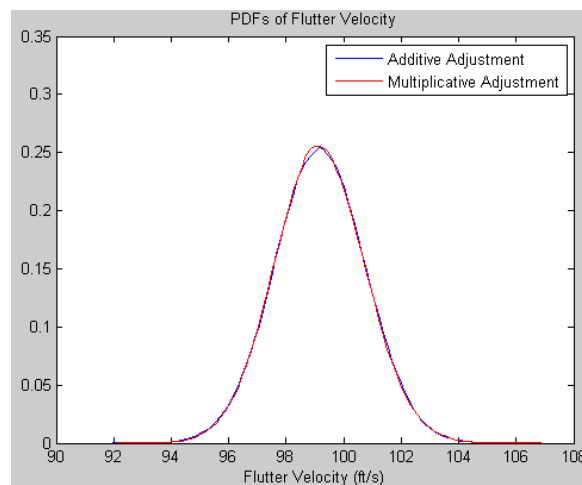


Figure 33: Normal and Lognormal Plots of V_f

As detailed above, the primary difference between multiplicative and additive adjustment factors approaches is the assumption of the final distribution. While in problems where the physical modeling is well understood and the variance between models is relatively small—such as the case shown above—the two approaches might result in similar distributions, in cases where the initial variance between models is large, the two approaches can produced dramatically different result. When such a case exists, existing knowledge regarding variable and model distributions must be used to decide upon an approach, or the two approaches must be analyzed individually.

The next step is to begin to quantify the model uncertainty in the problem, or more specifically, the uncertainty associated with the probabilities assigned to each of the models. By utilizing the probabilistic adjustment factors approach detailed in this research, the model probabilities, $P(M_i)$, can be assigned a distribution and the effect of their inherent uncertainty can be determined. By defining each of the four model probabilities as a normal distribution with a mean of their deterministic value, shown in Table 10, and a uniform standard distribution, the effect of model uncertainty can be calculated. With a standard deviation of 0.05 for each model probability distribution, the means and standard deviations of the final response output for flutter velocity were calculated and can be seen in Table 11.

Table 11: Distribution Parameters for Probabilistic Adjustment Factors Approach

	Mean	Standard Dev.
Additive	99.1753	1.4915
Multiplicative	99.1646	1.4867

By comparing the results of the deterministic and the probabilistic adjustment factors approach (Table 10 and Table 11), it can be seen that there is less than 0.1% percent difference between the two final distribution of flutter velocity for both the additive and multiplicative adjustment factors approach. This demonstrates that the effects of model uncertainty—the uncertainty in the model probabilities—are minimal for this problem, and that additional quantification of predictive uncertainty, such as by using posterior model probability updating, would be of minimal benefit in the reduction of the model uncertainty. This is valuable information for designers, as it provides information regarding the relative benefit and merit of conducting possibly expensive experiments to further refine and reduce model uncertainty. The results of this study would show to the designer that although there is uncertainty in the models being used, the introduction of new experimental data to the problem would not further reduce the model uncertainty.

6.0 OPTIMIZATION SCHEME

It is apparent how important of a role uncertainties play in RLV design and it is necessary to reduce the amount of risk. This can be accomplished by introducing an optimization scheme into the design of the RLV by minimizing risk. In most cases design optimization is thought to be based on a deterministic problem. Typically deterministic design optimization formulates the problem with an objective function that is to be minimized or maximized bounded by constraints which can be seen in Equations (46 - 48). The results to this optimization will consist of a single design point that satisfies the constraint conditions.

Minimize:

$$f(x) \tag{46}$$

Subject to:

$$g_i(x) \leq 0 \tag{47}$$

$$h_j(x) = 0 \tag{48}$$

In this case, x is the vector of design variables and $h_j(x)$ and $g_i(x)$ are equality constraints and inequality constraints respectively.

Reliability-Based Design Optimization (RBDO) is a valuable evolution in deterministic design optimization. Instead of optimizing a problem based on a deterministic problem the objective function is based on the probability of failure found using uncertainty quantification methods. Reliability-based design optimization accounts for these statistical distributions in the analysis through stochastic finite elements using FORM, SORM, evidence theory or many other reliability-based methods. RBDO formulates the problem with an objective function that is to be minimized or maximized bounded by constraints which can be seen in Equations (49 - 51).

Minimize:

$$P_f \quad (49)$$

Subject to:

$$g_i(x) \leq 0 \quad (50)$$

$$h_j(x) = 0 \quad (51)$$

In this case, x is the vector of design variables that can contain uncertainties or can influence uncertainties depending on how the problem is established. $h_j(x)$ and $g_i(x)$ are the same as in the deterministic design optimization problem. The objective function is now to reduce the probability of failure resulting in a highly reliable design.

Now that a basic understanding of reliability-based design optimization is understood an outline of the proposed design optimization of the RLV wing based on aeroelastic flutter simulation is explained. Due to the wide presence of uncertainty, as well as the different types of uncertainty present, accounting for uncertainty in the problem becomes necessary to perform a complete design. Figure 34 illustrates a flow chart of the propagation of uncertainties incorporated in an RBDO algorithm. In the RBDO section three methods will be explored; gradient-based RBDO, practical swarm optimization, and a proposed method of adaptive particle swarm optimization.

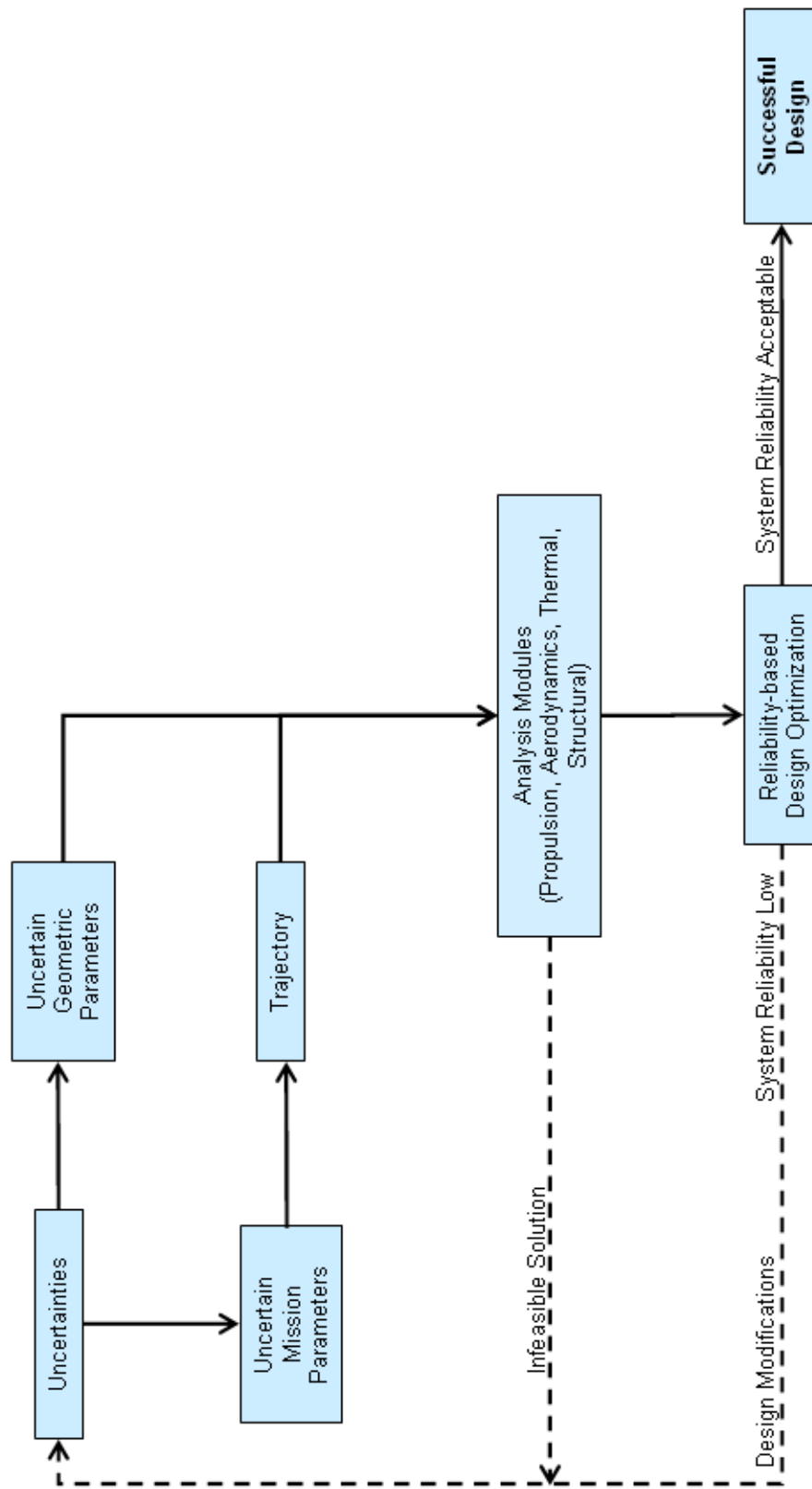


Figure 34: Vehicle Design Environment Framework

6.1 Reliability-Based Design Optimization Incorporating Evidence Theory

Reliability-Based Design Optimization (RBDO) techniques are developed to address the analytical guarantee of the performance of a structural system. In this section, uncertainty quantification using evidence theory demonstrated in the previous sections is implemented into design optimization. To address the discontinuity of the measurements (BEL and PL), a supplementary measurement, plausibility decision, described in section 5.3, will be used. The flow chart of gradient-based design optimization is demonstrated in Figure 35.

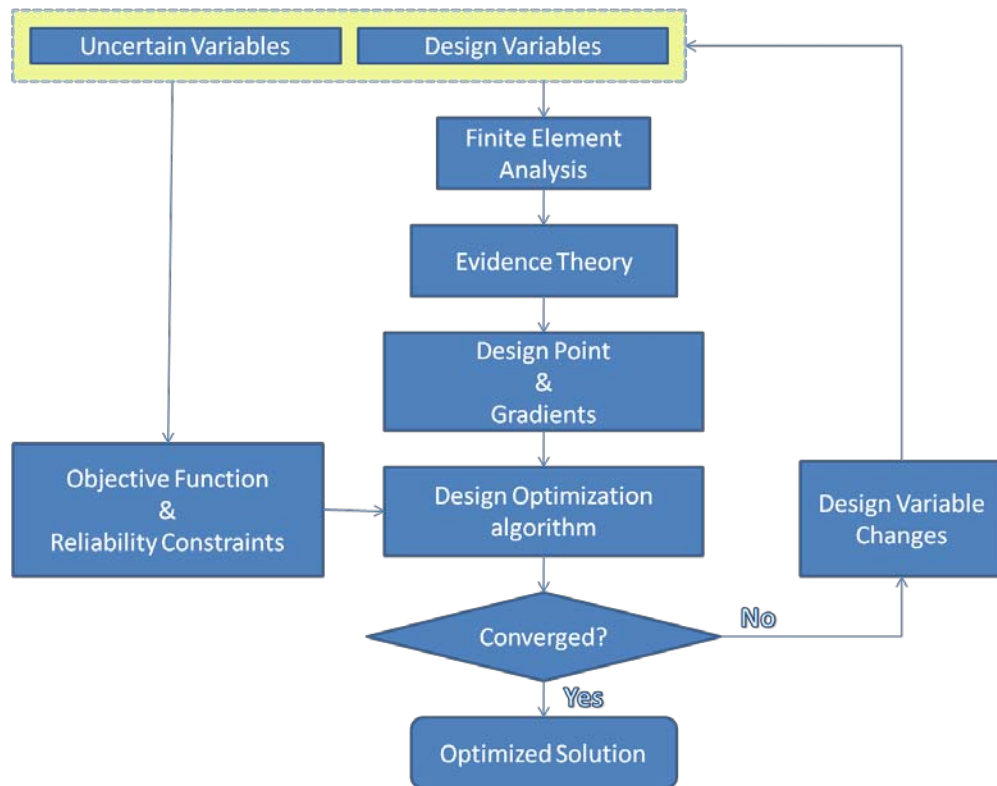


Figure 35: Gradient RBDO Flow Chart

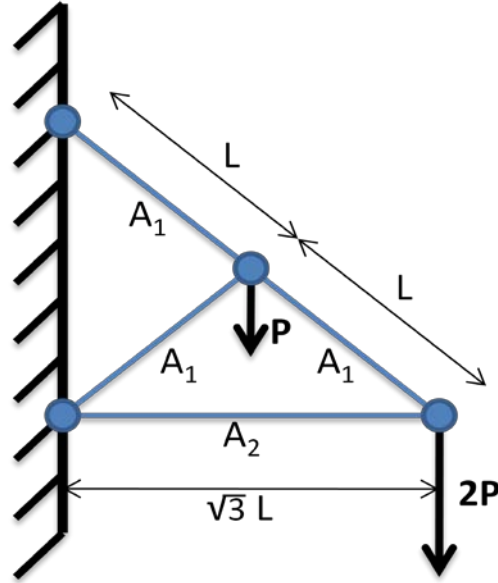


Figure 36: Four-Bar Truss Structure

As stated in section 5.3.1 the four-bar truss structure (Figure 36) will be revisited to investigate an RBDO analysis. To complete the design optimization portion of the analysis gradient information is needed to approximate the constraint function because no closed form equation can be derived when evidence theory is implemented. A surrogate model of the constraint was developed using TANA approximation (explained in section 5.2.1.) This approximation is only valid in short intervals the process outline in Figure 35 and requires iterations to get an accurate representation of the function.

The problem formulation for this example is as follows:

Minimize:

$$f = 3x_1 + \sqrt{3}x_2 \quad (52)$$

Subject to:

$$g_1 = 3 - \frac{18}{x_1} - \frac{6\sqrt{3}}{x_2} \geq 0 \quad (53)$$

$$g_2 = x_1 - 5.73 \geq 0 \quad (54)$$

$$g_3 = x_2 - 7.17 \geq 0 \quad (55)$$

$$drf - Pl_{dec} g1\ success \geq 0 \quad (56)$$

Where drf is the desired reliability factor for the constraint g_1 . drf is chosen by a designer based on how reliably they want the structure. Table 12 contains the results from the gradient-based RBDO using Benanazer's plausibility decision approximation. As seen in the table there are a range of optimizations, in which the drf was altered. The results show that since this problem was constrained with PL_{dec} rather than BEL or PL that the desired reliability factor was achieved in each analysis. Notice as the drf is increased (meaning reliability of the structure is increasing) the higher the objective function value is. This demonstrates a more reliable structure cost more materials than a less reliable one.

Table 12: Four-Bar Truss Reliability Design Optimization Results

f	x1	x2	drf	PL_dec	BEL	PL
43.52313	9.19752	9.19752	0	0	0	0.015
43.99996	9.335168	9.234402	0.01	0.01	0	0.0255
44.90086	9.423517	9.601514	0.1	0.1	0.015	0.253
45.26616	9.627671	9.458821	0.2	0.2	0.055	0.6095
45.44449	9.541425	9.711154	0.3	0.3	0.175	0.6095
45.62129	9.468467	9.939728	0.4	0.4	0.175	0.6195
45.78633	9.580633	9.839363	0.5	0.5	0.175	0.91
46.03484	9.682678	9.807335	0.6	0.6	0.53	0.917
46.35316	9.780256	9.822107	0.7	0.7	0.54	0.917
46.67998	9.785824	10.00115	0.8	0.8	0.54	1
47.18891	9.962875	9.988322	0.9	0.9	0.9	1
115.6673	23.78244	25.58815	0.95	0.95	0.9	1
152.1028	27.18551	40.57945	0.99	0.99	0.9	1
159.0244	26.79981	45.39415	1	1	1	1

6.2 Particle Swarm Optimization

Vehicle design is an inherently non-linear multi physical problem with the presence of continuous, mixed, and integer variables. To analyze the relative merit of a particular design, some degree of simulation required, and the time required for this simulation varies with the fidelity of the analysis required. In addition, the determination of design variable gradients is not analytically possible when simulation beyond basic static finite elements is employed.

Traditional gradient-based optimization methods rely on the input of design variable gradients, which would need to be determined using a finite-differencing scheme or analytical gradients—which are unavailable or difficult to obtain for many complex simulation analyses. Due to the relatively long simulation time required for an analysis, utilizing a finite differencing scheme can quickly become computationally restrictive. In addition, gradient-based methods perform very

poorly in highly non-linear problems, finding only local optima simply as a function of the initial design point.

Traditional heuristic methods, such as particle swarm optimization (PSO) help to alleviate some of these design problems [45]. PSO (Equations (57, 58)) is a heuristic method that will converge upon a global optimum and does not require gradient information at particular points.

$$v_{k+1}^i = wv_k^i + c_1r_1 \frac{p^i - x_k^i}{\Delta t} + c_2r_2 \frac{p_k^n - x_k^i}{\Delta t} \quad (57)$$

$$x_{k+1}^i = x_k^i + v_{k+1}^i \Delta t \quad (58)$$

However, as with most heuristic algorithms, PSO requires numerous function evaluations—often within a very small region of the design space—to converge upon an optimal point. In addition, due to the large number of user-controlled parameters in the optimization, the algorithm can perform much differently depending on the values of those inputs, which are based on the user's knowledge of the system at hand. Due to the lengthy simulation time required in vehicle design evaluations; this once again becomes computationally restrictive. When uncertainties within the design problem are introduced, the computational cost becomes even more restrictive, and traditional optimization methods become costly to the point of irrelevance.

In order to optimize the design of a proposed vehicle or vehicle component, these uncertainties listed above must be accounted for and an efficient algorithm must be able to

converge upon an optimum in an acceptable amount of time. With the introduction of uncertainties into the problem, the number of function evaluations required can increase dramatically. Ko et al [46] has previously used particle swarm to solve a trajectory optimization. Dimou et al also explored reliability-based optimal design of truss structures using particle swarm optimization [47]. Thus, a method must be implemented for the optimization routine that minimizes the number of function evaluations required while still converging upon an optimal solution.

The problem executed with this study is a closed form problem to stand as an initial surrogate for an actual vehicle design problem. This was done to limit the computational time required for an initial study, as the number of simulations required for each optimization can reach the thousands and a complete initial design space exploration was executed—meaning that nearly one million simulations would have been required for this initial study. The optimization problem executed for this was the “Egg Crate Function” (Equation (59)); a highly non-linear problem with multiple optima in a small region that is often used in the literature to explore the relative merit of optimization routines in highly non-linear design environments.

Minimize:

$$f(x) = x_1^2 + x_2^2 + 25(\sin(x_1)^2 + \sin(x_2)^2) \quad (59)$$

Subject to:

$$-2\pi \leq x_1 \leq 2\pi \quad (60)$$

$$-2\pi \leq x_2 \leq 2\pi \quad (61)$$

To initiate the design space, Latin Hypercube Sampling was used to span the entire design space with initial sampling points and ensure faster convergence. Figure 37 below shows a plot of the function and a sample iteration history for one of the optimizations of the “Egg Crate Function”.

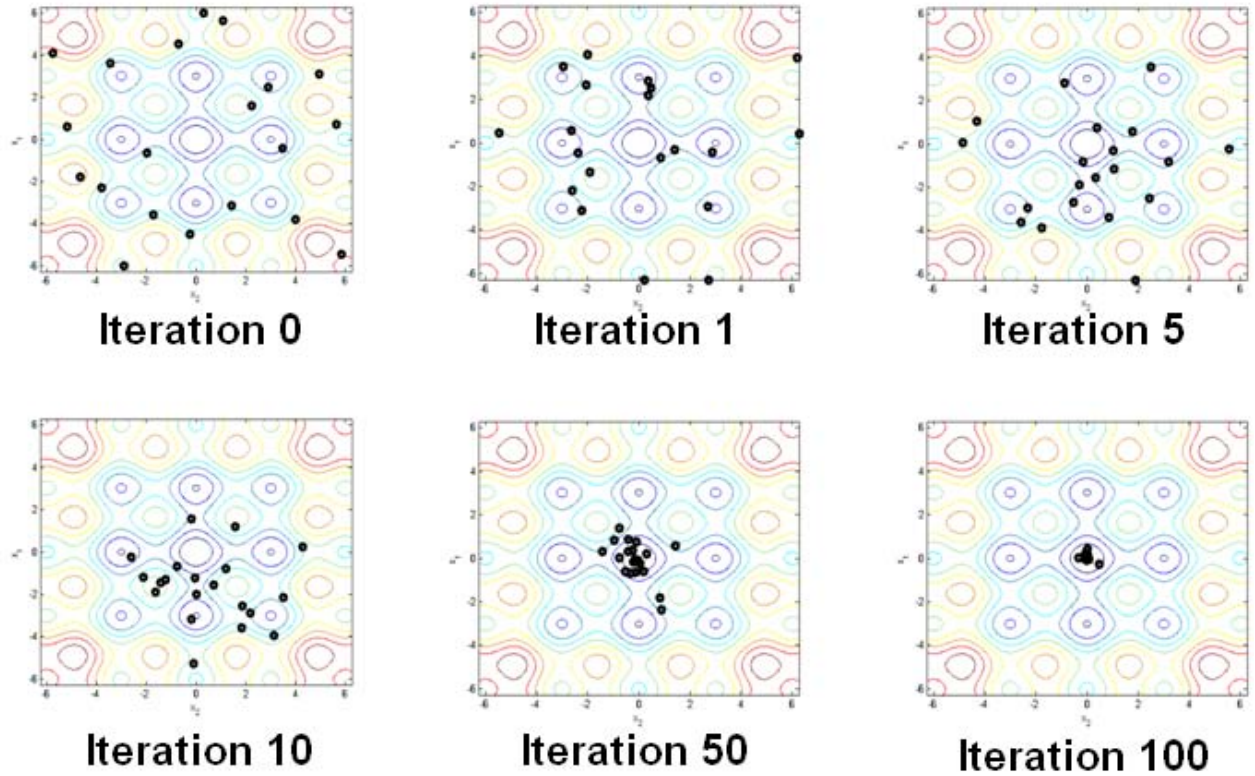


Figure 37: “Egg Crate Function” and Sample Iteration History

For this closed-form optimization problem, a design space study was conducted to determine the number of function evaluations—which directly correlate to the number of simulations required to analyze a vehicle’s performance—to converge upon an optimal solution. This included a study on the effect of the different parameters in particle swarm optimization to see how they affect the efficiency of the algorithm. For this study, ten different optimizations were executed at a baseline parameter set to establish an initial performance value Table 13. Then, individually, each controllable parameter was changed though the full spectrum of values to determine which parameters had significant effects on the efficiency of the algorithm. Plots of the number of simulations required for convergence versus the change in parameter values can be seen in Figure 38, Figure 39, Figure 40, and Figure 41. In addition, for the purpose of this initial study, only first-order variable interactions were explored.

Table 13: “Egg Crate Function” Optimization results at standard parameters

Num_part	Num_neigh	fw	w	c1	c2	y0	No. Fun. Calls
20	5	0.975	0.9	1.5	1.5	4.221E-08	940
20	5	0.975	0.9	1.5	1.5	4.158E-05	960
20	5	0.975	0.9	1.5	1.5	8.126E-05	900
20	5	0.975	0.9	1.5	1.5	7.949E-06	1000
20	5	0.975	0.9	1.5	1.5	6.730E-04	940
20	5	0.975	0.9	1.5	1.5	3.454E-04	1060
20	5	0.975	0.9	1.5	1.5	3.340E-05	1040
20	5	0.975	0.9	1.5	1.5	5.925E-04	980
						2.219E-04	977.5

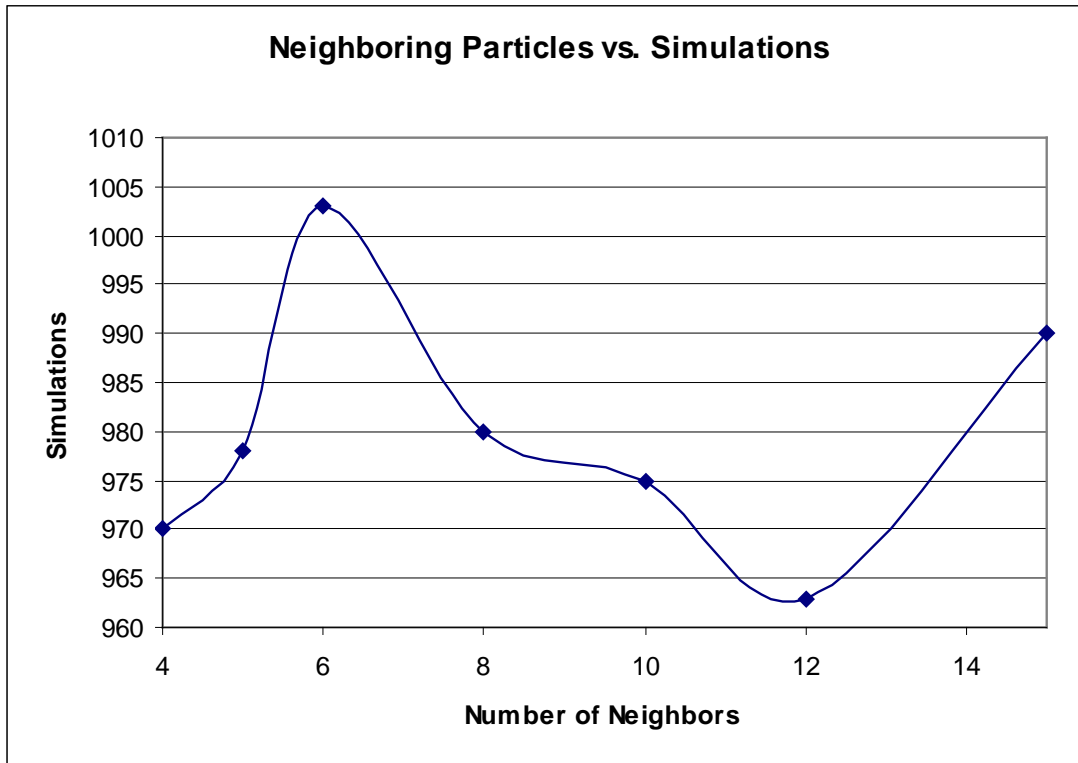


Figure 38: Number of Neighbors vs. Function Evaluations

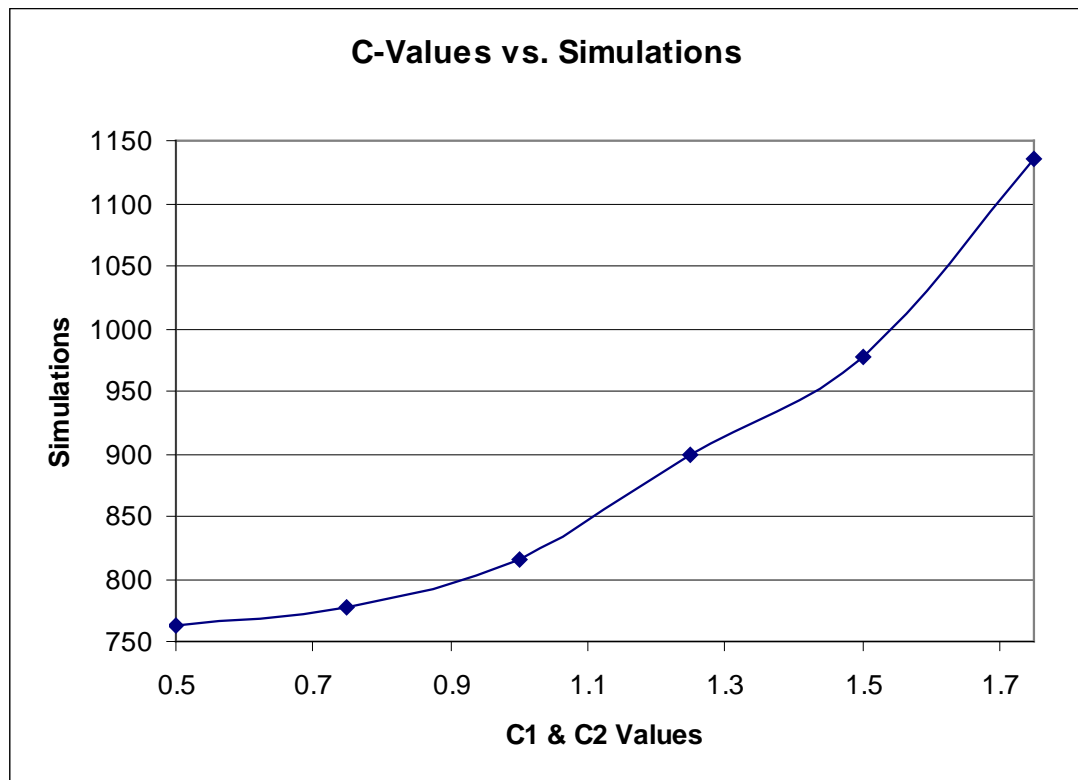


Figure 39: Individuality and Socialability Factors vs. Function Evaluations

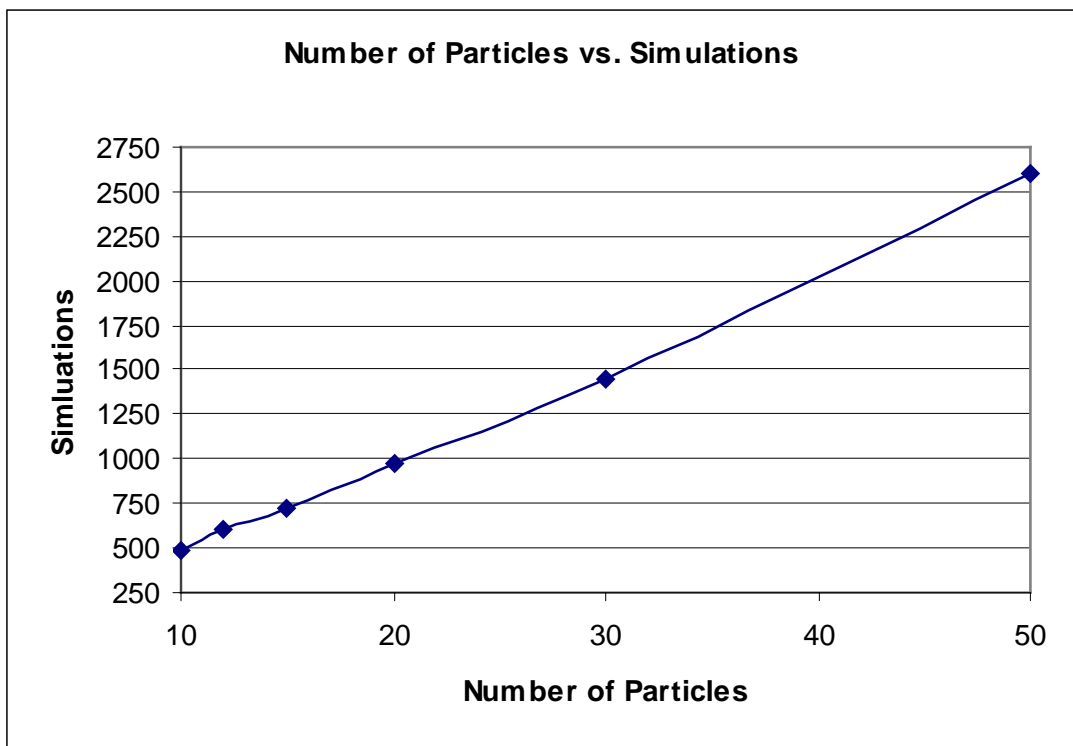


Figure 40: Number of Particles vs. Function Evaluations

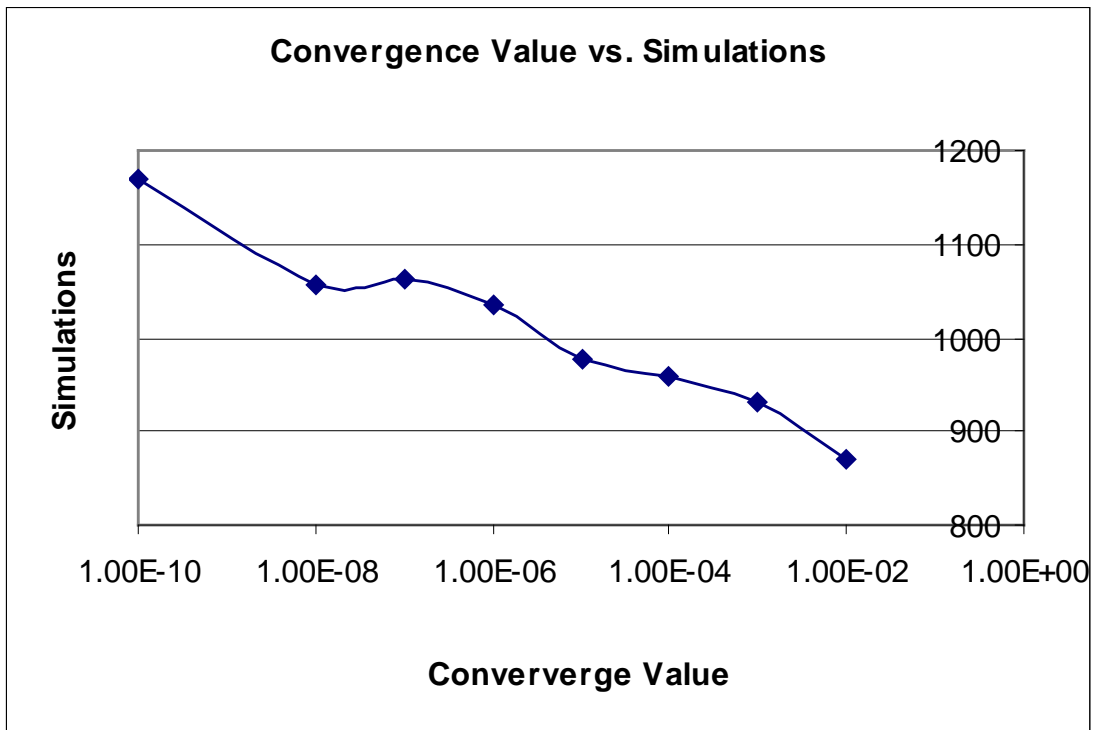


Figure 41: Convergence Value vs. Function Evaluations

It can be seen from these results that with traditional particle swarm optimization, some of the input parameters into the algorithm have dramatic effects upon the number of functions required for convergence. In addition to the data, the quality of the solutions that the algorithm converged to with different parameter values was recorded, but it was found that the quality of the solution was only a function of the convergence criteria, and not of any additional parameters in the problem.

After identifying significant input parameters in the conventional particle swarm algorithm, a modification was made to the algorithm in attempts to reduce the number of simulations required for convergence while still maintaining the desired level of accuracy. This method, called Adaptive Particle Swarm Optimization (A-PSO), is detailed in section 6.3.

6.3 Adaptive Particle Swarm Optimization (A-PSO)

As shown in the previous section, the computational cost for particle swarm optimization can be great. For a simple two-dimensional problem, it was shown that up to 1,000 simulations could be required for convergence, and this is before any degree of uncertainty is introduced into the problem—which as shown in previous sections could increase the number of simulations by a factor of 20 for a simple two dimensional problem. In addition, as greater dimensionality is added to the problem, these numbers scale exponentially; resulting in uncertain designs with only 5-6 design variables requiring upwards of 1,000,000 simulations for convergence using traditional particle swarm optimization. With detailed simulations, this number of required

simulations becomes prohibitively costly, and an alternative method must be found to reduce this number of simulations to a more manageable number.

While particle swarm optimization requires a large number of function evaluations to converge upon an optimal solution, it can be seen that a large number of these function evaluations occur within a small region of the design space. By implementing surrogate models in these small regions of the design space, the number of actual function evaluations can be dramatically reduced. However, when using surrogate modeling, there is an added error due to the inaccuracy of the model being implemented. In addition, if these models are considered valid over large regions of the design space, the error is increased. Thus, it can be seen that the small region of the design space that a surrogate model is considered valid, the more accurate it generally is. However, if the entire design space is simply partitioned into multiple small regions to be modeled with surrogate models, the number of simulations required to form these models would once again be large and unwieldy. Thus, what was done was to initiate traditional particle swarm optimization. The design space is then divided into several large regions to be modeled using a second order response surface model. Equation (62)

$$Y_j = \beta_o + \sum_{i=1}^n \beta_i X_{ji} + \sum_{i=1}^n \beta_i X_{ji}^2 + \sum_{i < j} \sum_p \beta_{ip} X_{ij} X_{jp} + \varepsilon_p \quad (62)$$

For the next iteration in the optimization, the function evaluations can then be approximated by the response surface models, which are considered valid within their region. Then, in order to add additional data into the models, a finite number of points (an additional parameter added to the traditional PSO algorithm) are randomly selected for full evaluation.

These points are fully evaluated—in the closed form problem this is rather simple, but in a simulation-based problem, this would represent additional simulations—and this new data is then used in conjunction with the existing points to update the surrogate models. When a region of the design space defined by a model becomes over-populated with function evaluations, the space is then partitioned into smaller regions, reducing the bounds on the models within that region. This can be best illustrated in Figure 42.

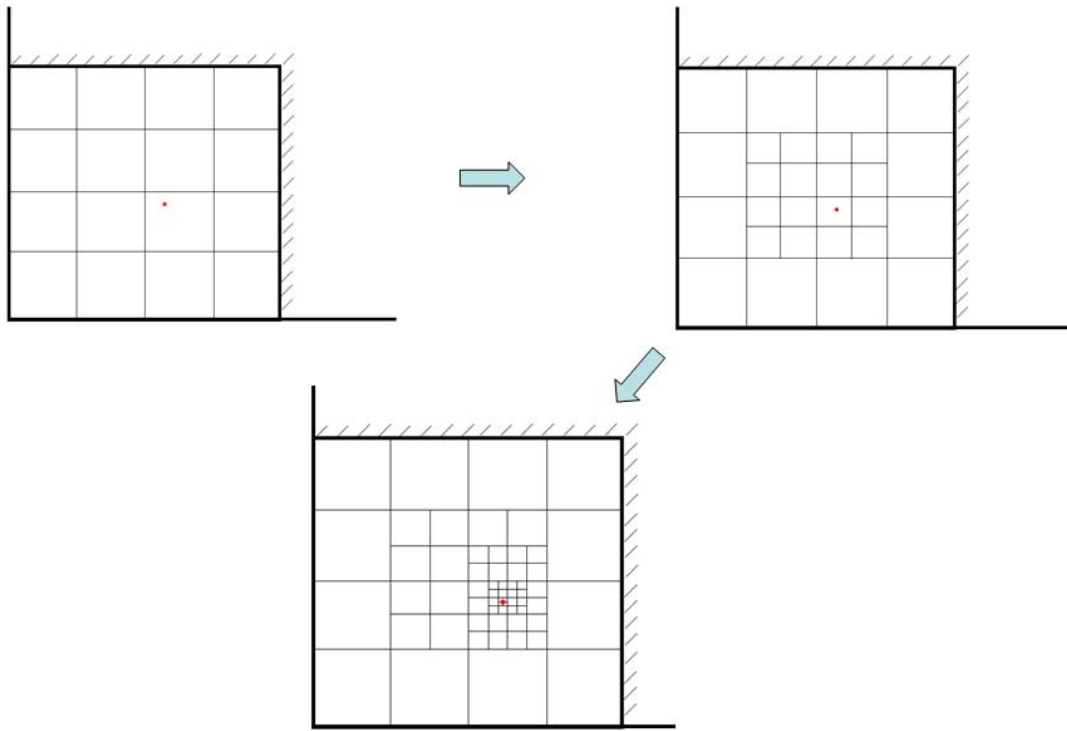


Figure 42: Model Design Space Reduction in A-PSO

This design space reduction is designed so that as the optimization algorithm converges upon a solution, the surrogate models become smaller and more numerous in the area of multiple particles, which corresponds to the location of an optimal solution. Thus, in this method, previous data regarding function evaluations is not wasted, but used to form surrogate models to aid in the convergence of the algorithm.

7.0 FAST WING RESULTS

7.1 Aleatory Uncertainty Investigation

To further investigate FORM and SORM for RLV design an aeroelastic model was analyzed with structural aleatory uncertainties. Using the model described in the chapter 4 an aeroelastic flutter uncertainty quantification analysis was investigated (Figure 43).

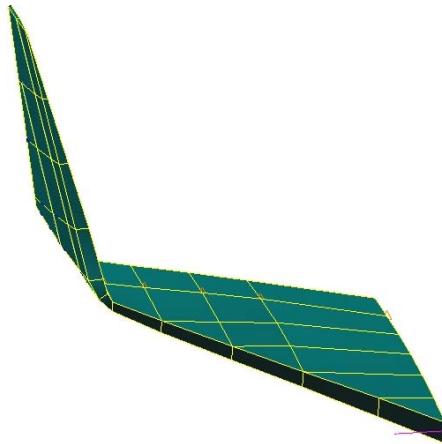


Figure 43: NASTRAN FEA Wing Model for Aleatory Risk Quantification Analysis

The two uncertain variables that were included in this analysis were selected to be the skin thickness and cross-sectional area of the wing. These variables are uncertain due to complex manufacturing process of composite materials. The parameters used for the atmospheric conditions in this analysis represent the vehicle entering the atmosphere during the trajectory at subsonic levels. The limit state allowed the flutter dynamic pressure to reach 2000 psf before it

was considered as a failure. The uncertain variables were represented by normal distributions. The means and standard deviations of the skin and spars cross-sectional area were $\mu=.04$ $\sigma=.005$ and $\mu=.2$ $\sigma=.02$ inches respectively. The results for the aleatory uncertainty quantification of the aeroelastic model are located in Table 14.

Table 14: Aleatory Uncertainty Quantification Results Including Aeroelastic Analysis

	Total Number of Function Calls	Total Computational Time	P_f	% Difference from MC
FORM with adaptive approximations	18	22 seconds	0.05075	.132
Breitung's Formulation	23	29 seconds	0.05082	.006
Tvedt's Formulation	23	29 seconds	0.05084	.045
Koyluoglu's Formulation	23	29 seconds	0.05066	.309
Monte Carlo	150,000	33.33 hours	0.05082	0

7.2 Epistemic Uncertainty Investigation

This study focuses on a reliability analysis of an RLV flutter speed. In past aerospace designs the vehicles were modeled without considering uncertainty which may have led to the Space Shuttle Challenger and the more recent Space Shuttle Columbia disasters. To quantify the uncertainties a more robust design can be implemented to the space program to avoid catastrophic events.

Epistemic uncertainty is a type of uncertainty where little information is known regarding the variable, and it would be inaccurate to assume some sort of distribution. Only epistemic uncertainties will be considered in this investigation. This problem will be formulated using non probabilistic methods since evidence theory is being incorporated. The uncertain variables are selected in this problem based on the little information known about the variable and the importance they play in the vehicle design. For example the composite skin on the RLV where two samples of the same composite can have completely different properties. This is related to the orientation of the layers. There is not enough information to construct a pdf on the orientation of each thus the variable is epistemic. Since RLV design consist of so many types of variables a limit state must be declared in order to complete an uncertainty analysis.

Flutter will be used as the limit state of this problem. In complex structures where both the aerodynamics and the mechanical properties of the structure are not fully understood the aeroelastic flutter phenomenon described in the previous section can be quantified with uncertainties. As seen in Figure 44 a demonstration of an uncertainty bound is added to the flutter assessment. This bound shows that if uncertainty is incorporated to an analysis it can cross the flutter margin causing catastrophic failure.

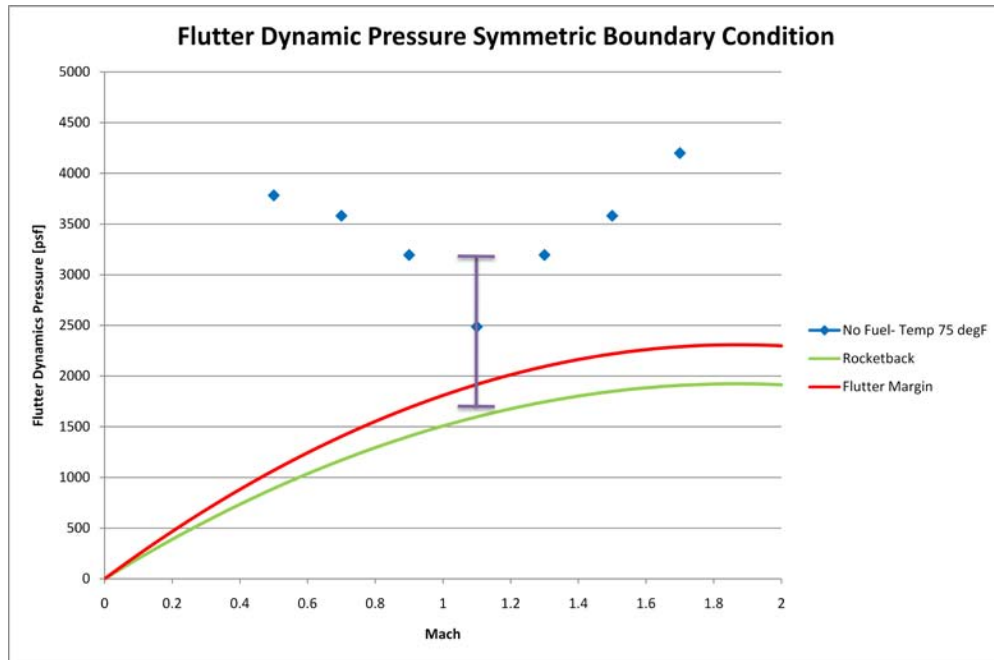


Figure 44: Aeroelastic Analysis with Uncertainty Bound

The variables that were chosen for this problem are based on two parts of the aeroelastic analysis to give diversity to the problem to demonstrate the coupling of uncertainties between the aerodynamic and structural model. The uncertainties come from the composites in the structural model and the atmospheric conditions in the aerodynamic model. As seen in Figure 45 on the left is the makeup of the composite material for the skin of the RLV and the right is the equation to calculate the air density. Composites have many uncertainties associated with them because they are hard to reproduce consistently. The uncertainties in the composite for this particular problem come from the thickness which can vary of the composite as well as the orientation of the third and fourth layer. These are considered epistemic uncertainties because there is not enough information on this type of composite to construct a pdf. The second group of uncertainties comes from the air density. The three uncertain variables associated with air density are the air pressure, gas constant, and temperature. The gas constant variable was selected to simulate

moisture in the atmosphere. The temperature and pressure were chosen because air pressure has a large dependence on them. The atmospheric conditions are thought to be epistemic uncertainty because there is not enough information to accurately construct a pdf without introducing more uncertainty into the problem.

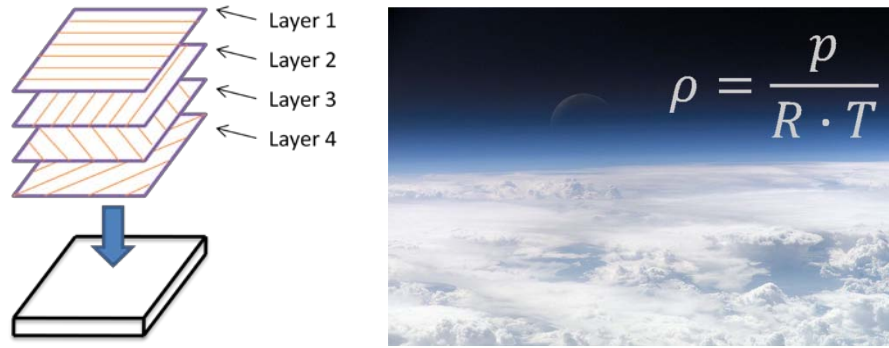


Figure 45: Uncertainties for six variables

Figure 46 represents the three uncertain variables BBA's for the composite uncertainties and Figure 47 signifies the three uncertain variables BBA's in the atmospheric uncertainties. In this problem three experts were asked their opinion on each variable, at which interval they thought the most likely occurrence of uncertainty would occur. Each interval was then weighted on the expert's opinion. Figure 46 and Figure 47 illustrates each expert's opinion in which for the variables layer thickness and temperature all three opinions were used. In the other four variables one expert did not express enough knowledge in that particular subject and the variable was omitted.

Composite Uncertainties

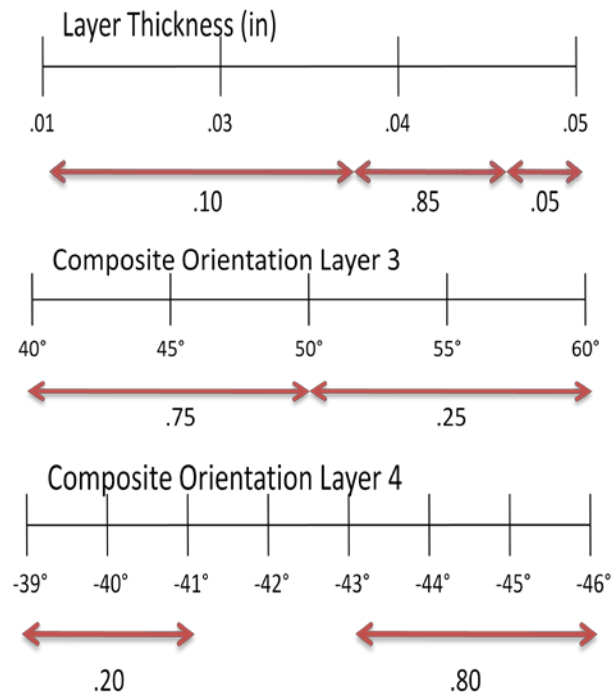


Figure 46: Composite Uncertainties Basic Belief Assignments

Atmospheric Uncertainties

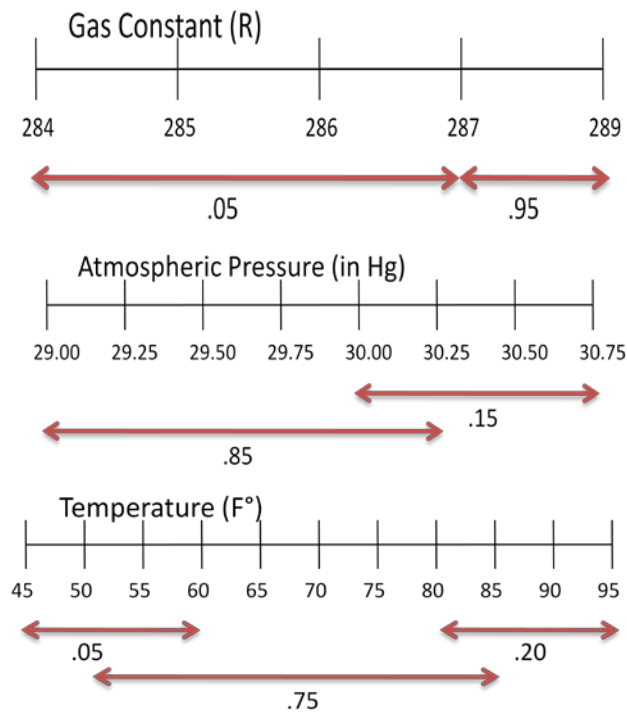


Figure 47: Aerodynamic Uncertainties Basic Belief Assignments

As mentioned in the two variable demonstration case, the limit state for the six variable problem is also 2000 psf. The results for the six variable problem are depicted in Figure 48. The reliability of the RLV falls between the bounds BEL and PL. This is expected since the RLV is initially designed to have a high reliability. The bounds can be improved to find a more accurate reliability and are explored in the next study.

$$\begin{aligned}
 BEL(A) &= \sum_{C \subset A} m(C) & PL(A) &= \sum_{C \cap A \neq \emptyset} m(C) \\
 BEL &= 0.925 & PL &= 1.0
 \end{aligned}$$

Figure 48: Six Variable RLV Problem Results

Simulations	3456
CPU time per simulation	30 sec
Total Time	28.8 hours

Figure 49: Simulation Time Six Variable RLV Problem

Figure 49 illustrates the efficiency of evidence theory. Although the method makes no assumptions and gives an accurate bound of the limit state the computational time is expensive. The more variables with uncertainty the more complex the problem becomes. As seen in the figure it took 28.8 hours to execute the analysis when each of the simulations took 30 sec to complete. This is why a model must have a short execution time otherwise the analysis would take years to complete. One possible solution would be to make a surrogate model of the aeroelastic flutter analysis such as a response surface which would look act like a closed form solution, resulting in a lower computational time. The problem with a surrogate model is it would introduce uncertainty to the problem which is trying to be avoided when using evidence theory.

The pay off of using evidence theory compared to a probabilistic method is no new uncertainty was added to the problem by assuming a pdf for the uncertain variables. If the wrong pdf was assumed and a probabilistic method such as first order reliability method or second order reliability method was used the reliability of the analysis could have deviated from the actual reliability causing misleading information.

There are two ways to improve the results of this type of analysis one being improving the BBA structures and the second by introducing the concept of Plausibility decision (PL_dec). If the plausibility belief bound is too large one solution is to further discretize the problem. This can be accomplished by improving the BBA structures. To improve the BBA's one can ask more experts, complete more experiments, or assume the expert opinions are evenly distributed and split them up into more pieces. Improving the BBA's structure will shrink the bound of the belief and plausibility giving a more understood problem.

One concern for an analysis with flutter is what if flutter does not occur during one of the iterations. Evidence theory does not use iterations so one simulation does not depend on the next. This works out very nicely when a simulation does not flutter. It can be considered as a successful case and the analysis could continue without penalty. For the current demonstration flutter occurred at every simulation

7.3 Reliability-Based Design Optimization Epistemic Uncertainty Investigation

Now that evidence theory has been demonstrated in the previous section it is apparent the probability of success can be improved. In this study an RLV wing structure will be optimized to reduce the weight while increasing the probability of success based on a flutter limit state.

The first step in the problem is to identify uncertainties. As mentioned before composite materials have uncertain properties and are hard to manufacture consistently. In the previous section the uncertainties came from the orientation of the layers of the composites that make up the skins of the wings. In this study only the composite thickness on the wings skin will be examined. Figure 50 contains images of the three sets of skin thicknesses that are being examined. The blue section will be referred to as the wing tip skin, the red portion will be recognized as the top skin, and the green segment will be identified as the bottom skin.

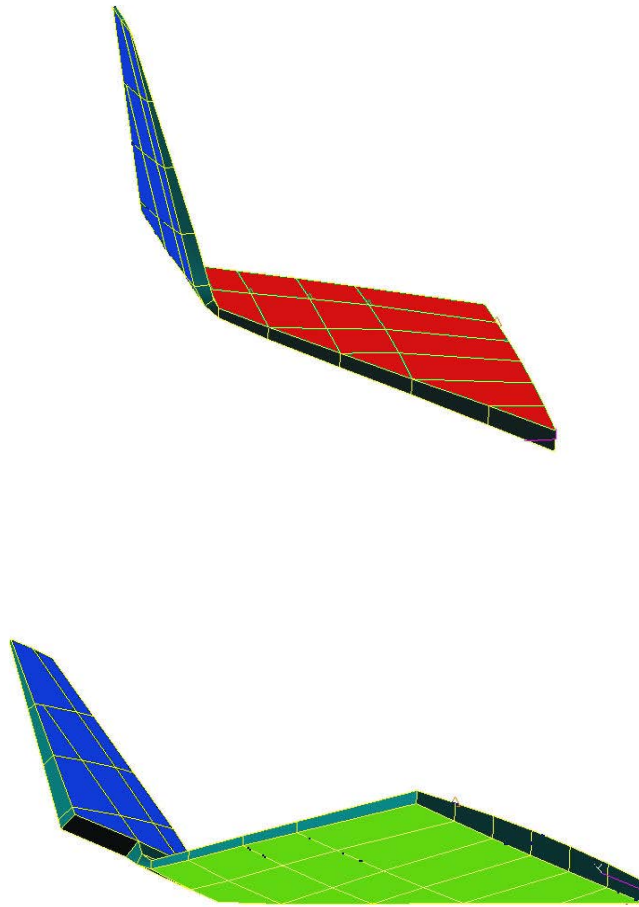


Figure 50: Variability Design of Skin Thickness Variables

This study also includes atmospheric density as an uncertainty. Like before the atmospheric density is an epistemic variable because there is not enough information to determine a well defined pdf. Instead of splitting the air density into an equation and three separate uncertain demonstrated in the previous section it will consist of only one uncertainty. This was done to reduce the computational time because now the problem is an iterative process and each additional uncertain variable increases computational time dramatically when employing evidence theory. The BBAs for the four uncertain variables can be found in Figure

51. Like before in the RBDO using evidence theory example the three skin thicknesses are distributed in percentages because not only will the skin thicknesses be the uncertainties in the, they will also be the design variables in which the problem is optimized.

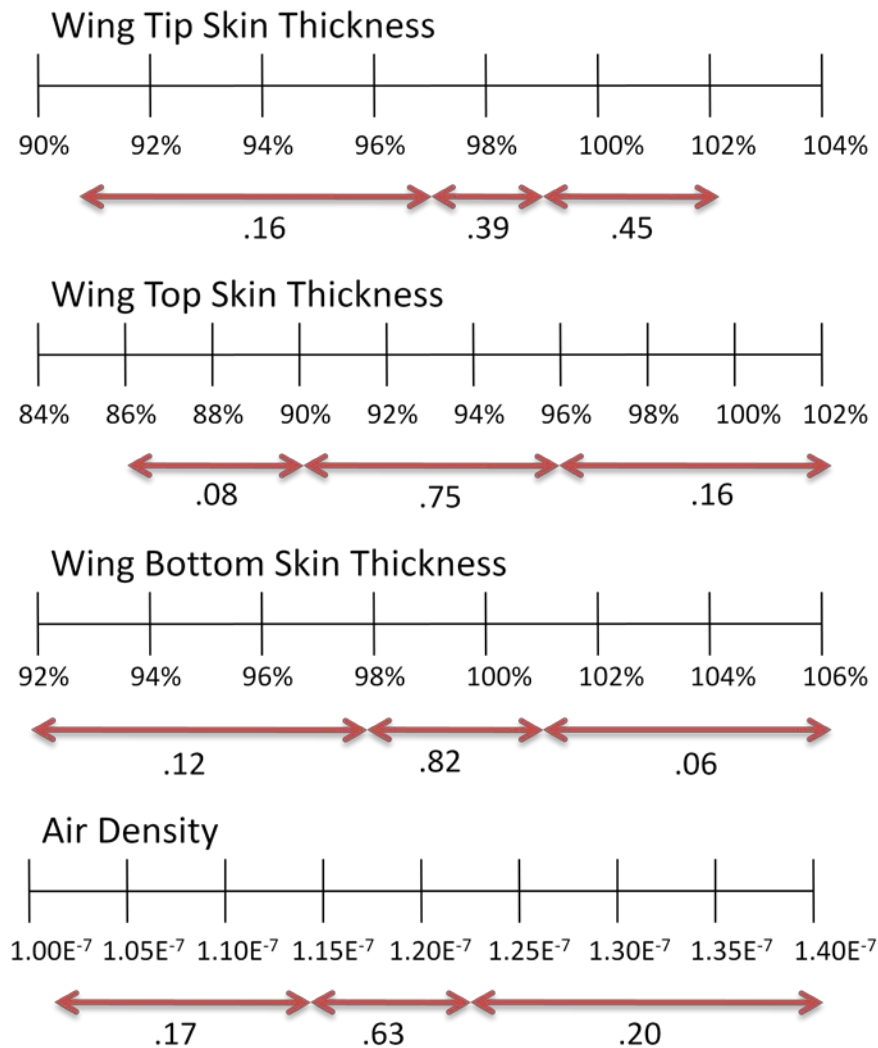


Figure 51: BBAs for the Wing structure used in the RBDO study

The BBAs were developed based on three expert opinions. Like in the evidence theory study of the RLV wing the limit state of the uncertainty quantification algorithm is flutter. While completing the evidence theory analyses during the RBDO, if a flutter dynamic pressure exceeds

2000 psf, it is considered a failure. The goal of the optimization is to minimize the weight (objective function, Equation (63)) of the wing while keeping a plausibility decision above .98.

Leading to the problem being defined as:

Minimize:

$$W = \sum_{i=1}^n \rho_i V_i \quad (63)$$

Subject to:

$$g_1 = \text{flutter limit state}(2000\text{psf}) \geq 0 \quad (64)$$

$$drf - Pl_{dec} \text{ } g1 \text{ success} \geq 0 \quad (65)$$

Where n is the number of elements that consist of the skin section. ρ_i and V_i are the mass density and volume, respectively, of the i^{th} structural element participating in the design. drf is the desired reliability factor which in this case is .98.

Table 15 shows the initial and optimized results for the RLV wing optimization. The optimization resulted in an increase in PL_dec and Belief while reducing the weight of the wing. The optimization converged at 15 iterations. Figure 52 shows the computational time invested in this RBDO.

Table 15: RBDO Wing Thickness Results

	Wing-Tip skin (in)	Wing-top skin (in)	Wing-Bottom skin (in)	Weight (lb)	PL_dec	PL	BEL
Initial	0.0576	0.144	0.0536	769.78	0.9175	0.99	0.786
Optimized	0.0488	0.132	0.0632	766.5072	0.98	0.99	0.8242

Iterations	15
CPU time per Iteration	8 hours
Total time	120 hours

Figure 52: Simulation Time RBDO Analysis

8.0 DISCUSSION AND CONCLUSIONS

The technical effort conducted in this task developed methods relevant to the reliability-based structural design of an RLV. The first step completed in the analysis of the RLV wing was a trajectory optimization for a rocket-back mission, where it was discovered that critical points in the trajectory needed further investigation. From the mission's trajectory, critical points were selected based on maneuverability and rapid changes in atmospheric conditions.

To evaluate these critical points, a finite element model was needed. The wing model was based on representative dynamic characteristics of the RLV configuration. Since no physical model of the RLV wing is available, the created wing model was validated based on the original model using two methods of characteristics validation. The two methods used were the modal assurance criterion for mode shape comparisons and frequency comparison analysis. From these analyses we concluded that the two models compared are in sufficient agreement that the created model can be used as a surrogate. Along with the structural model an aeroelastic model was constructed in which a series of flutter analyses were conducted. These analyses were based on a flight envelope during the launch phase of the trajectory. This regime was selected because the RLV experienced the most dynamic pressure during this phase. From this study it was determined that the critical Mach number relating to the flutter speed was at Mach 1.1.

Once the model was validated and finalized, uncertainty quantification methods were explored. Three sources of uncertainty were explored in this research: aleatory, epistemic, and model-form. It was discovered that when quantifying aleatory uncertainties, the second-order

reliability method produces better results than the first-order reliability method at the cost of more computational time. Epistemic uncertainty was analyzed using evidence theory where uncertain variables with limited information were quantified. This resulted in bounds of actual response. A new metric known as plausibility decision was introduced to estimate the reliability within the bound and to obtain gradient information. Three methods of plausibility decision were investigated, and Benanzer's approximation was determined to be the most fitting for an evidence theory analysis with more than two variables. This effort also produced a new method to quantify model-form uncertainty. This type of uncertainty is present when more than one type of model is available for an analysis, such as finite element models with different fidelities or using different computational methods.

The next step in this investigation was incorporating uncertainty quantification into the design optimization. Gradient-based reliability-based design optimization incorporating evidence theory was utilized. It was discovered that in reliability-based design problems, gradient information is extremely computationally expensive. The computational cost arises from finding the gradients where the number of simulations needed in the reliability analysis is the number of variables plus one. An adaptive particle swarm optimization program was developed to reduce this computational time.

Finally, three separate analyses were completed on the RLV wing incorporating uncertainties. The first was an aleatory uncertainty quantification incorporating structural uncertainties and an aeroelastic flutter limit state. This analysis discovered that the FORM and SORM methods produced results with nearly the same reliabilities. This indicates that the limit

state is nearly linear when only structural parameters are used in an aleatory investigation. The second analysis conducted was an evidence theory uncertainty quantification analysis, where the uncertainties were found in atmospheric conditions and composite materials. For this study six uncertain variables were used, three of which came from structural uncertainties and three from atmospheric uncertainties. Flutter dynamic pressure was used as the limit state. This investigation concluded that when epistemic uncertainties were considered a wider reliability bound was obtained. A wider bound implied the need for additional information about uncertain parameters. Although a high reliability was determined, it was still necessary to perform a risk minimization optimization. The third analysis conducted was a gradient-based reliability design optimization of the RLV wing including aeroelastic uncertainties. The uncertain variables were three sections of skin thicknesses as well as air density. The design variables in the optimization were the three skin sections thicknesses, where the objective function was to minimize weight. The optimization of the RLV wing demonstrated that a reduction in weight as well as an increase in reliability could be obtained through optimal modification of thickness distributions.

9.0 BIBLIOGRAPHY

- [1] Jategaonkar R., Behr R., Gockel W., and Zorn C., "Data Analysis of Phoenix Reusable Launch Vehicle Demonstrator Flight Test," *Journal of Aircraft*, vol. 43, no. 6, pp. 1732-1732, 2006.
- [2] Cook S., "NASA's Integrated Space Transportation Plan — 3rd Generation Reusable Launch Vehicle Technology Update.," *Acta Astronautica*, vol. 53, no. 4-10, pp. 719-728, 2003.
- [3] Shaw E.J., "RLV Economics: Fiscal Evaluation of NASA's Reusable Launch Vehicle Effort," *Space Policy*, vol. 13, no. 2, pp. 109-124, 1997.
- [4] Sietzen F.J., "The Quest for Reusability," *Aerospace America*, vol. 46, no. 9, pp. S26-S31, 2008.
- [5] Deneu F., M., Malassigne, Le-couls O., and Baiocco P., "Promising Solutions For Fully Reusable Two-Stage-To-Orbit Configurations," *Acta Astronautica*, vol. 56, no. 8, pp. 729-736, 2005.
- [6] Kaplan M.H., "Reusable Launch Vehicle Facts and Fantasies," *AIP Conference Proceedings*, vol. 608, no. 1, pp. 1181-1186, 2002.
- [7] Xu Y., "Trajectory Analysis for Vertical Takeoff and Vertical Landing Reusable Launch Vehicle's Upper Stage," *Journal of Aerospace Engineering*, vol. 22, no. 1, pp. 58-66, 2009.
- [8] Berend N. and Talbot C., "Overview of Some Optimal Control Methods Adapted to Expendable and Reusable Launch Vehicle Trajectories," *Aerospace Science & Technology*, vol. 10, no. 3, pp. 222-232, 2006.
- [9] Nelson D., "Qualitative and Quantitative Assessment of Optimal Trajectories by implicit Simulation (OTIS) and Program to Optimize Simulated Trajectories (POST)," April 26, 2001.
- [10] Powell R.W., "Program to Optimize Simulated Trajectories (POST 2)," *Users Manual, Version 1.1.6.G*, vol. II, 2003.
- [11] Allemang R.J., "The Modal Assurance Criterion - Twenty Years of Use and Abuse," *Sound and Vibration*, no. August, pp. 14-21, 2003.
- [12] Lang G.F., "Experimental FEA. Much more Than Pretty Pictures!," *Sounds and Vibration*, no. January, pp. 12-20, 2005.
- [13] Friedmann P.P., McNamara J.J., Thuruthimattam B.J., and Nydick I., "Aeroelastic analysis of hypersonic vehicles," *Journal of Fluids & Structures*, vol. 19, no. 5, pp. 681-712, 2004.
- [14] Thuruthimattam B.J., Friedmann P.P., McNamara J.J., and Powell K.G., "Modeling approaches to hypersonic aeroelasticity," in *ASME International Mechanical Engineering Congress and Exposition*, New Orleans, Louisiana, 2002.
- [15] Kanda A., Tetsuhiko U., and Takashi K., "Flutter Characteristics of Reentry Space Vehicle with Nonplanar Wing," *AIAA*, vol. 44, no. 10, pp. 2267-2267, 2006.
- [16] Johnson E.H. and Rodden W.P., *MSC/NASTRAN Version 68 Aeroelastic Analysis Users Guide.*: The MacNeal-Schwendler Corporation, 1994.

- [17] Rüdiger R., "Reliability Analysis - Past, Present and Future," in *8th ASCE Specialty Conference on Probabilistic Mechanics and Structural Reliability*, 2000.
- [18] Kiureghian A. D. and Ditlevsen O., "Aleatory or Epistemic? Does it Matter?," *Structural Safety*, vol. 31, pp. 105-112, 2009.
- [19] Kurdi M., Lindsley N., and Beran P., "Uncertainty Quantification of the Goland Wing's Flutter Boundary," in *AIAA Atmospheric Flight Mechanics Conference and Exhibit*, Hilton Head, SC, 2007.
- [20] Petit C.L., "Uncertainty Quantification in Aeroelasticity: Recent Results and Research Challenges," *Journal of Aircraft*, vol. 41, no. 5, pp. 1217-1229, 2004.
- [21] Pradlwarter H.J. et al., "Realistic and Efficient Reliability Estimation for Aerospace Structures," *Computer Methods in Applied Mechanics and Engineering*, vol. 194, no. 12-16, pp. 597-617, 2005.
- [22] Petit C.L and Grandhi R.V., "Optimization of a Wing Structure for Gust Response and Aileron Effectiveness Reliability," *Journal of Aircraft*, vol. 40, pp. 1185-1191, 2004.
- [23] Drogue E.L. and Mosleh A., "Bayesian Methodology for Model Uncertainty Using Model Performance Data," *Risk Analysis*, vol. 28, no. 5, pp. 1457-1476, 2008.
- [24] Cheng J., Cai C.S., Xiao R.C., and Chen S.R., "Flutter Reliability Analysis of Suspension Bridges," *Journal of Wind Engineering*, vol. 93, pp. 757-775, 2005.
- [25] Bae H.R., Grandhi R.V., and Canfield R.A., "An Approximation Approach for Uncertainty Quantification Using Evidence Theory," *Reliability Engineering and System Safety*, vol. 86, pp. 215-225, 2004.
- [26] Bae H.R., Grandhi R.V., and Canfield R.A., "Epistemic Uncertainty Quantification Techniques Including Evidence Theory for Large-Scale Structures," *Computers and Structures*, vol. 82, pp. 1101-1112, 2004.
- [27] T. Ueda, "Aeroelastic Analysis Considering Structural Uncertainty," in *Proceedings of the Sixth International Seminar on "Recent Research and Design Progress in Aeronautical Engineering and its Influence on Education"*, vol. IX, Riga, Latvia, 2005, pp. 3-7.
- [28] Yan-Gang Z. and Tetsuro O., "A General Procedure for the First/Second-Order Reliability Method (FORM/SORM)," *Structural Safety*, vol. 21, pp. 95-112, 1999.
- [29] Hasofer A.M. and Lind N.C., "Exact and Invariant Second-Moment Code Format," *J Engrg Mech Division, ASCE*, vol. 100, no. 1, 1974.
- [30] Wang L. and R.V. Grandhi, "Improved Two-Point Function Approximations for Design Optimization," *AIAA Journal*, vol. 33, no. 9, pp. 1720-1727, 1995.
- [31] Breitung K., "Asymptotic Approximations for Multinormal Integrals," *Journal of the Engineering Mechanics Division*, vol. 110, no. 3, pp. 357-366, 1984.
- [32] Tvedt L., "Two Second-order Approximations to the Failure Probability," in *Section on Structural Reliability*, Hovik, Norway, 1984.
- [33] Koyluoglu H. U. and Nielsen S. R. K., "New Approximations for SORM Integrals," *Structural Safety*, vol. 13, pp. 235-246, 1994.
- [34] Dempster A. P., "A Generalization of Bayesian Inference," *Journal of the Royal Statistical Society*, vol. 30, no. Series B, pp. 205-247, 1968.
- [35] Shafer G., "A Mathematical Theory of Evidence," *Princeton University Press*, 1976.

- [36] Bae H.R., Grandhi R.V., and Canfield R.A., "Uncertainty Quantification of Structural Response Using Evidence Theory," *AIAA Journal*, vol. 41, no. 10, pp. 2062-2068, 2003.
- [37] Bae H.R., Grandhi R.V., and Canfield R.A., "Sensitivity Analysis of Structural Response Uncertainty Propagation Using Evidence Theory.," *The Journal of the International Society for Structural and Multidisciplinary Optimization*, 2003.
- [38] Alyanak E., Grandhi R., and Bae H.R., "Gradient Projection for Reliability-Based Design Optimization Using Evidence Theory," *Engineering Optimization*, vol. 40, no. 10, pp. 923-935, 2008.
- [39] Benanzer T., "System Design of Undersea Vehicles," Wright State University, Dayton, PhD Dissertation 2008.
- [40] Haftka R. and Gurdal Z., "Elements of Structural Optimization Third Revised and Expanded Edition," *Kluwer Academic Publishers*, 1992.
- [41] Leamer E.E., *Specification Searches: Ad hoc Inference with No Experimental Data*. New York, New York: Wiley & Sons, 1978.
- [42] Mosleh A. and Apostolakis G., "The Assessment of Probability Distributions from Expert Opinions with an Application to Seismic Fragility Curves," *Risk Analysis*, vol. 6, no. 4, pp. 447-461, 1986.
- [43] Zio E. and Apostolakis G., "Two Methods for the Structural Assessment of Model Uncertainty by Experts in Performance Assessments of Radioactive Waste Repositories," *Reliability Engineering & System Safety*, vol. 54, no. 2-3, pp. 225-241, 1996.
- [44] Reinert J.M. and Apostolakis G.E., "Including Model Uncertainty in Risk-Informed Decision Making," *Annals of Nuclear Energy*, vol. 33, no. 4, pp. 354-369, 2006.
- [45] Kennedy J. and Eberhart R. C., "Particle Swarm Optimization," *Proceeding of IEEE Conference on Neural Network*, vol. 4, pp. 1942-1948, 1995.
- [46] Ko C. N., Yang C. C., and Wu C. J., "A Particle Swarm Optimization Based Time-Scaling Method for Quasi Time-Optimal Control of Rigid Spacecraft Along Specified Paths," *Proceedings of the Institution of Mechanical Engineers -- Part I -- Journal of Systems & Control Engineering*, vol. 222, no. 1, pp. 1-9, 2008.
- [47] Dimou C. K. and Koumoussis V. K., "Reliability-Based Optimal Design of Truss Structures Using Particle Swarm Optimization," *Journal of Computing in Civil Engineering*, vol. 23, no. 2, pp. 100-109, 2009.